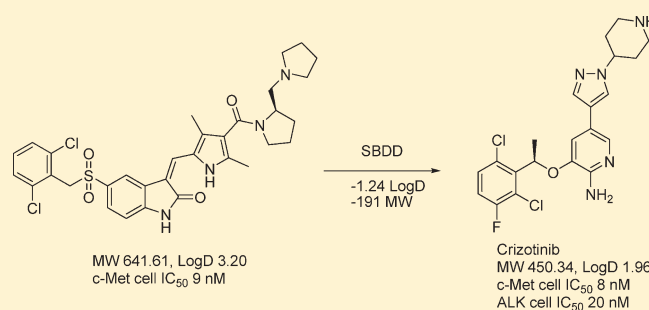


Structure Based Drug Design of Crizotinib (PF-02341066), a Potent and Selective Dual Inhibitor of Mesenchymal–Epithelial Transition Factor (c-MET) Kinase and Anaplastic Lymphoma Kinase (ALK)[†]

J. Jean Cui,* Michelle Tran-Dubé, Hong Shen, Mitchell Nambu, Pei-Pei Kung, Mason Pairish, Lei Jia, Jerry Meng, Lee Funk, Iriny Botrous, Michele McTigue, Neil Grodsky, Kevin Ryan, Ellen Padrique, Gordon Alton, Sergei Timofeevski, Shinji Yamazaki, Qihua Li, Helen Zou, James Christensen, Barbara Mroczkowski, Steve Bender, Robert S. Kania, and Martin P. Edwards

La Jolla Laboratories, Pfizer Worldwide Research and Development, 10770 Science Center Drive, San Diego, California 92121, United States

ABSTRACT: Because of the critical roles of aberrant signaling in cancer, both c-MET and ALK receptor tyrosine kinases are attractive oncology targets for therapeutic intervention. The cocrystal structure of **3** (PHA-665752), bound to c-MET kinase domain, revealed a novel ATP site environment, which served as the target to guide parallel, multiattribute drug design. A novel 2-amino-5-aryl-3-benzoxypyridine series was created to more effectively make the key interactions achieved with **3**. In the novel series, the 2-aminopyridine core allowed a 3-benzoxo group to reach into the same pocket as the 2,6-dichlorophenyl group of **3** via a more direct vector and thus with a better ligand efficiency (LE). Further optimization of the lead series generated the clinical candidate crizotinib (PF-02341066), which demonstrated potent in vitro and in vivo c-MET kinase and ALK inhibition, effective tumor growth inhibition, and good pharmaceutical properties.



INTRODUCTION

Receptor tyrosine kinases (RTKs) play fundamental roles in cellular processes, including cell proliferation, migration, metabolism, differentiation, and survival. RTK activity is tightly controlled in normal cells. The constitutively enhanced RTK activities from point mutation, amplification, and rearrangement of the corresponding genes have been implicated in the development and progression of many types of cancer.¹ Successful approval of small molecule tyrosine kinase inhibitors has clinically validated this mode of therapeutic intervention, along with several pathogenic tyrosine kinases as effective molecular targets for cancer therapy. Recent examples include imatinib in gastrointestinal stromal tumors with mutant c-KIT kinase or chronic myelogenous leukemia with BCR-ABL gene translocations, erlotinib in non-small-cell lung cancer (NSCLC) with mutant EGFR, and sunitinib targeting the VHL-dependent VEGF pathway in renal cell carcinoma.

Signaling from the receptor tyrosine kinase c-MET, also known as hepatocyte growth factor receptor (HGFR), and its natural ligand hepatocyte growth factor (HGF), also known as scatter factor, plays important roles during normal development, organogenesis, and homeostasis. After activation by HGF,

c-MET induces an invasive program consisting of cell proliferation, migration, invasion, survival, and branching morphogenesis. Aberrant c-MET signaling through constitutive activation, gene amplification, and mutations occurs in virtually all types of solid tumors and is implicated in dysregulation of multiple tumor oncogenic processes such as mitogenesis, survival, angiogenesis, invasive growth, and especially the metastatic process.² Furthermore, the overexpression of c-MET and HGF was demonstrated to correlate with poor prognosis or metastatic progression in a number of major human cancers.³ For these reasons c-MET and its ligand HGF have become leading candidates for molecular targeted cancer therapies.

Anaplastic lymphoma kinase (ALK) is a receptor tyrosine kinase, grouped together with leukocyte tyrosine kinase (LTK) to a subfamily within the insulin receptor (IR) superfamily. ALK was first discovered as a fusion protein, NPM (nucleophosmin)–ALK in anaplastic large cell lymphoma cell lines in 1994.⁴ The transforming ability of NPM–ALK was demonstrated, and the oncogenesis requires the activation of ALK kinase function as a result of oligomerization mediated by the NPM segment.⁵ ALK with other chromosomal rearrangements have been detected in anaplastic large cell lymphoma (50–60%), inflammatory myofibroblastic tumors (27%), and non-small-cell lung

[†] PDB codes are the following: 2wkm for the PHA-665752/c-MET complex; 2wgj for the PF-02341066/c-MET complex; 2xp2 for the PF-02341066/ALK complex.

Received: June 13, 2011

Published: August 03, 2011

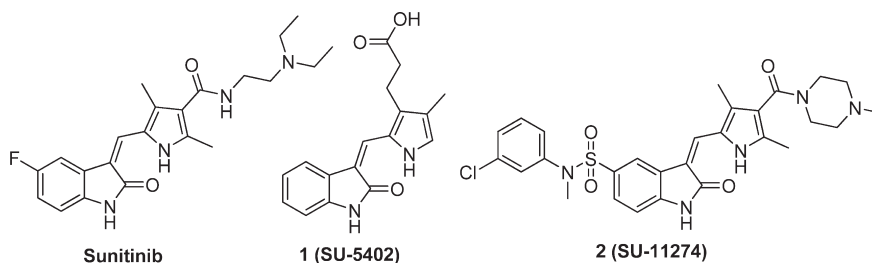


Figure 1. Structures of kinase inhibitors.

cancer (4–7%).⁶ The ALK fusion proteins have a common structural feature with the amino terminal region of the fusion protein containing an oligomerization domain to cause the oligomerization of the fusion protein and ALK kinase-mediated autophosphorylation. EML4–ALK fusion gene, comprising portions of the echinoderm microtubule associated protein-like 4 (EML4) gene and the ALK gene, was first discovered in non-small-cell lung cancer archived clinical specimens and also cell lines.⁷ EML4–ALK fusion variants were demonstrated to transform NIH-3T3 fibroblasts and cause lung adenocarcinoma when expressed in transgenic mice, which confirm the potent oncogenic activity of the fusion kinase.⁸ Oncogenic mutations of ALK in both familial and sporadic cases of neuroblastoma have also been reported.⁹ Therefore, ALK is an attractive molecular target for cancer therapeutic intervention.

Herein, we detail the drug design campaign that led to crizotinib (PF-02341066, **63**), a potent and selective c-MET/ALK dual inhibitor.¹⁰ Consistent with its mechanism of action, crizotinib demonstrates dose-dependent inhibition of phosphorylation of c-MET, NPM–ALK, and selected variants, as well as targets dependent functions in tumor cells both in vitro and in vivo.¹⁰ Crizotinib showed antitumor efficacy, including marked cytoreductive antitumor activity, in multiple tumor models implanted in athymic mice that expressed activated c-MET or ALK fusion proteins.¹⁰ In additional published studies, crizotinib inhibits tumor cell growth of cell lines harboring fusion variants and activating mutations of ALK including Karpas299 (NPM–ALK), SU-DHL-1 (NPM–ALK), Kelly neuroblastoma (active ALK mutation), and NCI-H3122 (EML4–ALK variant 1) with IC_{50} values ranging from 74 to 544 nM.¹¹ On the basis of an exceptional attribute profile, crizotinib was advanced into human clinical studies for the treatment of cancer.

RESULTS AND DISCUSSION

Foundations of Structure Based Design. To enable a structure based drug design (SBDD) program, a kinase domain (KD) construct of c-MET, in its nonphosphorylated form, was prepared for utilization in cocrystallization experiments. Fortunately, cell-based activity of the inhibitors prevented RTK autophosphorylation, consistent with inhibitory interaction with the nonphosphorylated form in cells. Inhibition of phosphorylated c-MET KD in purified enzyme biochemical assays confirmed that the inhibitors can inhibit both unactivated and activated c-MET. Overall, there was little divergence between enzyme and cell data, apart from that which could be readily understood by permeability/efflux considerations. Where there was minor divergence, the structural biology was illuminating, as will be discussed below.

The search for leads started in a potent class of kinase inhibitors, the 3-substituted indolin-2-ones, where one representative,

sunitinib, is now approved for GIST and RCC treatment.¹² The selectivity of indolin-2-ones for particular kinases is mediated by substituents built onto the indolin-2-one core. Both 4-substituted indolin-2-ones and 5-substituted indolin-2-ones were evaluated for c-MET inhibition and attractive lead matter was found.¹³ From this starting point, key cocrystal structures guided both prioritization decisions and drug design strategy.

To monitor the progress of optimization, lipophilic efficiency ($LipE = pK_i$ (or pIC_{50}) – $cLogD$) was used as a numerical index of binding effectiveness.¹⁴ Drug design aimed at improvement of LipE results in parallel optimization for desirable ADME and greater likelihood of safe drug profiles, since ligand interactions with most proteins are substantially influenced by lipophilicity.¹⁵ This convenient numeric index that reflects compound target potency relative to lipophilicity is presented consistently throughout, demonstrating the effectiveness of integrated SBDD and property based drug design.

c-MET Leads from the 3-Substituted Indolin-2-one Series. Compound **2** (SU11274), shown in Figure 1, was identified as a c-MET inhibitor with isolated enzyme IC_{50} of 10 nM.¹⁶ **2** inhibited HGF-induced c-MET autophosphorylation in a dose dependent manner with complete inhibition at 1 μ M in A549 c-MET cellular assay.¹⁶ Optimization of **2** led to **3** (PHA-665752) (Figure 4), a c-MET RTK inhibitor with a significantly improved cellular potency ($IC_{50} = 9$ nM in GTL-16 cell line) and selectivity (>50-fold for c-MET compared with a panel of diverse tyrosine and serine–threonine kinases).^{13c,17} **3** was broadly used in preclinical studies to build confidence in c-MET as a target for cancer therapy and to identify potential patient populations.¹⁸ In a variety of tumor cells, **3** potently inhibited HGF stimulated and constitutive c-MET phosphorylation, downstream signal transduction of c-MET, and HGF/c-MET driven phenotypes, e.g., cell growth, cell motility, invasion, and morphology. In vivo, **3** inhibited c-MET phosphorylation in tumor xenografts, and tumor growth in a dose-dependent manner.^{17,18} However, the poor pharmaceutical properties of **3** limited its further development as a clinic candidate.¹⁹

A cocrystal structure of **3** bound to the unphosphorylated c-MET KD revealed the key binding interactions as presented in Figure 2 (PDB code 2wkm). In the complex of **3**, the c-MET KD adopts the unique autoinhibitory conformation observed previously in crystal structures of the apo-enzyme and a complex with the staurosporine analogue K252a.²⁰ In these c-MET crystal structures, the beginning of the kinase activation loop (residues 1222–1227) forms a turn that wedges between the β -sheet and the α C-helix. Consequently, the activation loop significantly displaces the α C-helix from a catalytically competent position and the downstream activation loop residues (1228–1245) to a position that interferes with ATP and substrate binding. This unusual kinase activation loop conformation creates a unique

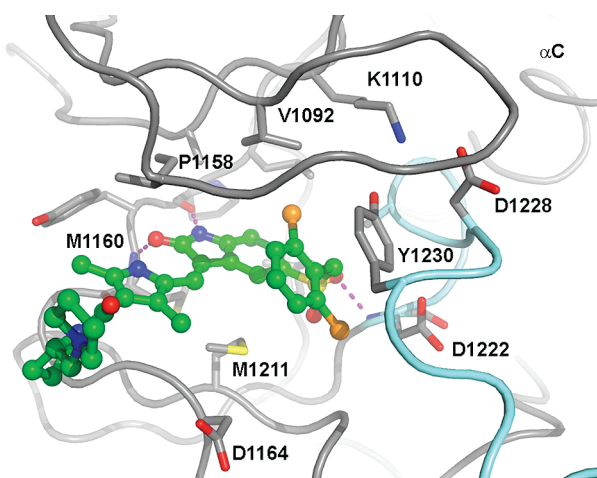


Figure 2. Cocrystal structure of **3** bound to the kinase domain of c-MET. The backbone trace of the activation loop is highlighted in cyan, and hydrogen bonds are indicated as dashed lines.

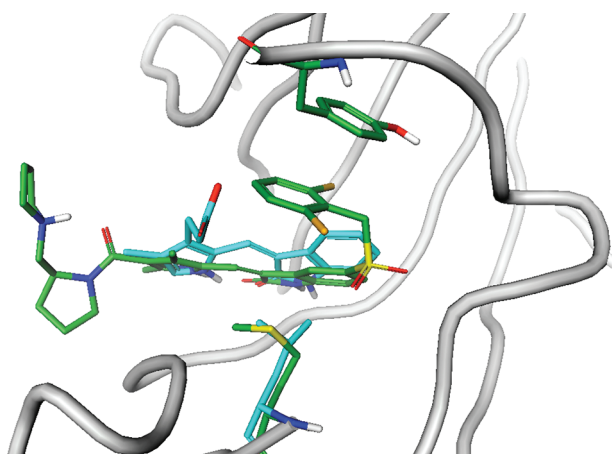


Figure 3. Structure overlay of **3**/c-MET (green/gray) and **1**/FGFR1K (cyan).

inhibitor binding pocket which presents an opportunity for the design of selective inhibitors.

As in a previously published cocrystal structure of **1** (SU5402) with fibroblast growth factor receptor 1 kinase (FGFR1K),²¹ the oxindole ring N–H and carbonyl oxygen of **3** form two hydrogen bonds to the protein backbone of the kinase hinge region. Also, similar to the **1**/FGFR1K complex, the amide substituent off the pyrrole ring extends into the solvent surrounding the kinase hinge segment. For both inhibitors, the oxindole and pyrrole rings are in a coplanar conformation, stabilized by resonance and an intramolecular hydrogen bond between the pyrrole N–H and the oxindole O=C. This flat scaffold provides strong interactions to the adenine binding cleft while fitting its flat dimensions well. Unlike the **1**/FGFR1K structure, the plane of the oxindole–pyrrole system in **3** is tilted away from the c-MET glycine-rich loop significantly (down in Figure 3), a difference arising from both protein and inhibitor structural differences. This lower inhibitor position in c-MET is permitted by the more flexible (and compressed) Met-1211 and is stabilized by the critical π – π stacking interaction between the benzyl group and Tyr-1230 of the A-loop in its unique conformation (Figure 2). A hydrogen

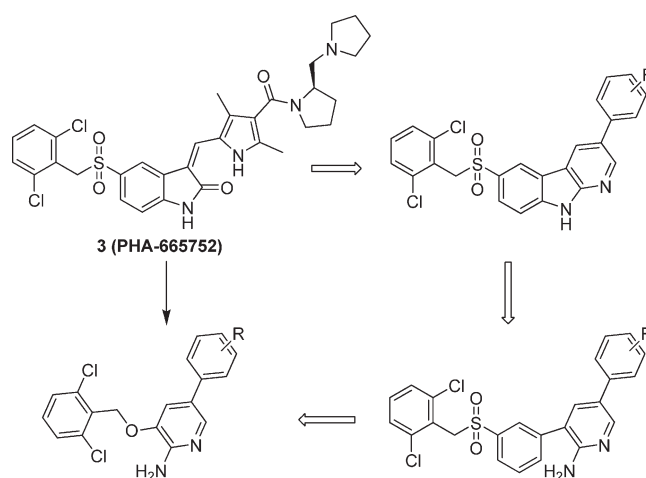


Figure 4. Design of 5-aryl-3-benzyloxy-2-aminopyridine scaffold for c-MET inhibition.

bond between the oxygen of the sulfonyl group and the backbone N–H of Asp-1222 is also stabilizing this orientation.

For clarity, it is useful to establish that all the inhibitors discussed herein are believed to bind the above unique A-loop conformation of c-MET and that the phosphorylation state of c-MET protein in different contexts is as follows: (1) c-MET remains nonphosphorylated in cells when inhibited; (2) in crystal structures of nonphosphorylated c-MET the protein adopts a unique conformation to which the inhibitors bind. It is also recognized that phosphorylation of the activation loop is part of the regulatory mechanism that destabilizes the autoinhibited activation loop conformation that is serving as the drug design target. Impacts of this become apparent in small potency trend differences between enzyme and cell assays for certain inhibitor structural types. The differences arise, predictably, from structural features optimized to bind adjacent to the activation loop.

Design of Novel 5-Aryl-3-benzyloxy-2-aminopyridine c-MET Inhibitors. Although **3** demonstrated potent and selective inhibition of c-MET autophosphorylation and related biological functions in both in vitro and in vivo studies, the poor pharmaceutical properties (low solubility, high metabolic clearance, and poor permeability) limited further development for human clinical studies. With improved pharmaceutical properties as the goal, a key strategy was to design smaller and less lipophilic inhibitors (**3**, MW = 641.62, measured log *D* = 3.20 at pH 7.4, c-MET cell IC₅₀ = 9 nM, LE = 0.25,²² LipE = 4.85) with good kinase selectivity.

The cocrystal structure of **3** with c-MET KD was analyzed to elucidate opportunities to make key interactions with a more efficient use of chemical structure. Starting with fundamental scaffold optimization, one such opportunity was recognized by analyzing the indolin-2-one pyrrole core, which extends the full length of the adenine pocket. In addition to occupying a low tilt position in the adenine pocket (vide supra) the core size requires that the sulfone methylene linker make a U-turn to position the 2,6-dichlorophenyl group for a π – π stacking interaction with Tyr-1230. Consequently, a significant portion of the indolinone ring along with the sulfone linker was identified as inefficient scaffolding for the 2,6-dichlorophenyl group. Compounds were designed with a smaller hinge binder, from which could be positioned an aryl ring to interact with Tyr-1230 in a more direct manner.

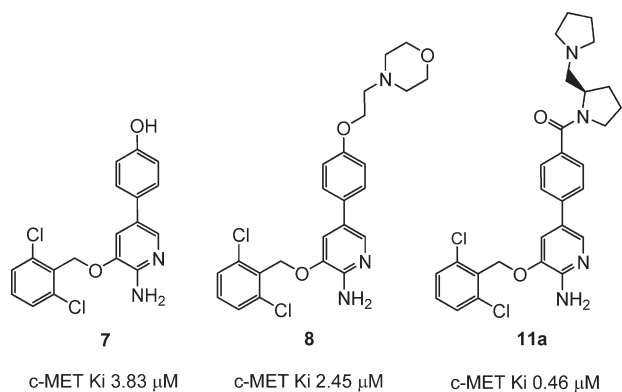


Figure 5. First iteration 2-aminopyridines show c-MET inhibition.

Through re-engineering of the central core rings (three iterations of thinking are depicted in Figure 4), the novel 5-aryl-3-benzyloxy-2-aminopyridine scaffold was designed. This required a recentering and truncating of the pyrrole–oxindole platform down to a small, adenine-pocket core. Accordingly, the 2-aminopyridine NH and ring nitrogen were expected to make H-bonds to the hinge protein residues Pro-1158 and Met-1160, similar to the oxindole ring of **3**. The more bold requirement of this design is that the 3-benzyloxy group must take an efficient path, along a new vector, to stack with Tyr-1230. For the shortened linkage to stretch back to the hinge, binding must be accompanied by a scaffold tilt back to the higher adenine pocket position seen with **1**. Last, the aryl group at the 5-position of this new scaffold is easily anticipated to point toward solvent in the same way oxindole–pyrrole substituents do, providing a handle to modulate lipophilicity.

The design concept was tested with a small set of compounds shown in Figure 5. Compound **7** displayed moderate inhibition against c-MET with an enzymatic K_i of 3.83 μ M (LE = 0.29, LipE = 0.35). The introduction of a 2-morpholinoethoxyethyl group in **8** showed a similar potency against c-MET as **7**. Although this is less efficient, retained inhibition is consistent with the 5-phenyl group pointing toward solvent and the 2-aminopyridine interacting at the hinge. Compound **11a** (LE = 0.24, LipE = 3.70), with the same amide group as **3**, demonstrated improved absolute potency against c-MET and also LipE value, again consistent with a similar binding mode for this novel series. Additionally, given the different binding vector of the new series, optimal substituents for the novel 2-aminopyridines were not expected to mirror those of the oxindole core. A cocrystal structure of the 2-aminopyridine core making H-bonds to the hinge confirmed the adenine binding orientation.²³ For compounds **7**, **8**, and **11a**, the structural features that are necessary to bind the hinge backbone were incorporated in the monocyclic 2-aminopyridine whereas the *O*-methylene-2,6-dichlorophenyl was intended to fully and efficiently interact with Tyr-1230 of the A-loop. The trajectory of the solvent exposed group and the electronic effects already observed between **8** and **11a** gave reason to expect that optimization from this point would be productive. From this novel series, with greater promise of efficiency, optimization was focused on improving c-MET potency and physical properties in parallel.

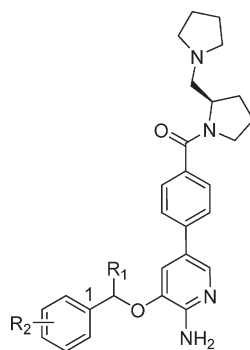
Optimization of the 3-Benzyloxy Group. Further optimization of the 2-aminopyridine series was supported by the promising inhibition exhibited by **11a**, which also served as a convenient scaffold for initial analogues. According to the binding mode of the original design hypothesis, the benzyloxy group at the

3-position is the structural feature that binds to the hydrophobic pocket and interacts with Tyr-1230, a priority area to study structural modifications. Various aryl analogues intended to interact with Tyr-1230 were targeted, with representative results and LipE analysis results summarized in Table 1 and Figure 6. The convenience of the graphical plot allows for easy recognition of overall optimization against constant LipE zones, facilitating the mining of structural features that impart movement orthogonal to the LipE lines (e.g., **14c**, **14i**, and **14j** are similarly efficient across broad potency/cLogD space).

Unsubstituted **11b** serves as a benchmark for c-MET kinase inhibition (K_i = 7.92 μ M, LipE = 3.66), establishing a baseline to analyze LipE contributions from different phenyl ring substitution patterns. The relatively conservative phenyl ring derivatives displayed in Table 1 have enzymatic LipE values ranging from 3 to 5. The 2-position, monosubstituted phenyl ring compounds **14a–d** had measurable increases in potency against c-MET, with the exception of nitrile **14c**. Although with potency similar to that of **11b**, this nitrile compound had the highest biochemical LipE of 4.31. However, **14c** was not active in the c-MET cellular assay at 10 μ M tested. Compound **14e**, a 4-position derivative bearing the highly lipophilic *tert*-butylphenyl group, had improved enzymatic potency against c-MET (K_i = 0.98 μ M). However, the lower LipE (3.15), which was even worse when using cell-based numbers, indicated that the potency gain was not attractive relative to lipophilicity cost. The 2,4-dichloro substituted compound **14f** showed slightly improved enzymatic LipE due to a lower lipophilicity. This translated to greater cell potency with an IC_{50} of 0.41 μ M and one of the three big jumps in cell LipE observed within this table. Although a number of variables could be contributing, the cell vs biochemical potency of **14f** was an early indication that SAR between cell and biochemical measures may diverge because of the different binding affinity of the inhibitor to nonphosphorylated c-MET vs phosphorylated c-MET. Importantly, cell/enzyme potency divergence was associated with the benzylic structural feature, which interacts with the unique tyrosine and protein conformation of nonphosphorylated c-MET discussed earlier. Previous work with RTKs reinforced the practice of targeting nonphosphorylated kinase and prioritizing the cell-based data, which is consistent with conformations and interactions seen crystallographically.²⁵ The potency contribution of the 3-fluoro substituent on the phenyl ring was demonstrated by **14h** compared to **14g**. The addition of the 3-fluoro imparted a 5-fold increase in enzymatic potency (K_i = 0.88 μ M) and a 14.5-fold increase of cell potency (IC_{50} = 0.56 μ M) relative to the 2-chloro-6-fluorophenyl ring of **14g** (K_i = 5.11 μ M and cell IC_{50} = 8.12 μ M). The improvement of c-MET cell LipE, from 3.45 to 4.38 for **14h**, reinforced the importance of this single atom change and is the second jump in LipE. Overall, the phenyl group substitution optimization provided moderate improvement to c-MET potency, with notable impacts for 2-chloro and 3-fluoro substitution.

Further optimization came from modification to the linkage between the 2-aminopyridine core and the phenyl ring just discussed. A small lipophilic pocket, visible to the upper left of Figure 3, is adjacent to the putative bound location of the 3-benzyloxy linker. Adding small lipophilic bulk to this structural feature led to enhanced efficiency from an α -methyl group. As demonstrated with compounds **14i–k**, inclusion of the α -methyl group boosted both enzymatic and cell potencies significantly compared with the desmethyl analogues, justifying the added lipophilicity. By comparison of the α -methyl **14j** with the desmethyl analogue **11a**, the

Table 1. Structure–Activity Relationship of Substitutes on 3-Benzyloxy Group



compd	R ₁	R ₂	cLogD ^a	c-MET K _i (μM) ^b	LipE(K _i) ^c	c-MET cell IC ₅₀ (μM) ^b	LipE(IC ₅₀) ^c
11a	H	2,6-di-Cl	2.64	0.46	3.70	1.79	3.11
11b	H	H	1.44	7.92	3.66	>10.0	<3.56
14a	H	2-F	1.49	2.82	4.08	6.62	3.69
14b	H	2-Cl	2.03	1.71	3.79	5.85	3.20
14c	H	2-CN	0.88	6.50	4.31	>10.0	<4.12
14d	H	2-CF ₃	2.01	2.59	3.58	7.11	3.14
14e	H	4- <i>tert</i> -butyl	3.13	0.98	3.15	8.53	1.94
14f	H	2,4-di-Cl	2.64	1.03	3.35	0.41	3.75
14g	H	2-Cl-6-F	1.64	5.11	4.16	8.12	3.45
14h	H	2-Cl-3,6-di-F	1.87	0.88	4.18	0.56	4.38
14i	CH ₃	2-Cl-3,6-di-F	2.22	0.26	4.37	0.39	4.19
14j	CH ₃	2,6-di-Cl	2.99	0.068	4.20	0.14	3.86
14k	CH ₃	2,6-di-Cl-3-F	3.10	0.012	4.82	0.020	4.60

^a Calculated logarithm of the octanol/water distribution coefficient at pH 7.4 using ACD pchbat, version 9.3. ^b Inhibition constants (K_i)²⁴ and cell IC₅₀^{10a} were determined as described in Experimental Methods. The coefficients of variance were typically less than 20% (*n* = 2). A549 human lung carcinoma cell line was used for the evaluation of the inhibition of autophosphorylation of c-MET. ^c LipE = pK_i (or pIC₅₀) – cLogD.

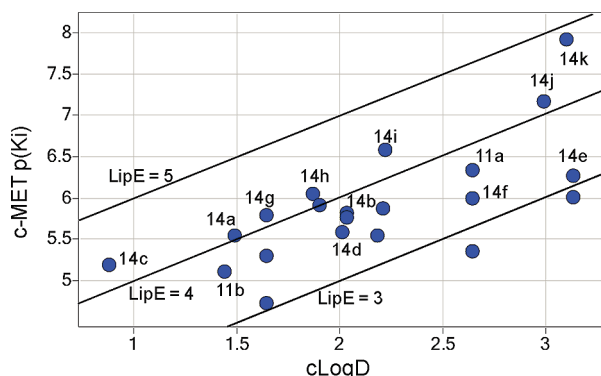
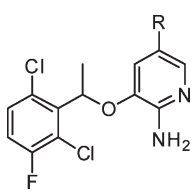


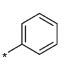
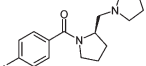
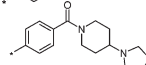
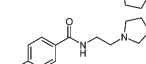
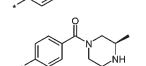
Figure 6. LipE plot highlights **14k**, **14i**, and **14c** as lead compounds and where close analogues reside.

enzyme based LipE improves from 3.70 to 4.02 and the cell-based LipE improves from 3.11 to 3.86. Importantly, bringing together the 2,6-dichloro and 3-fluoro and α -methyl into a single compound, **14k**, resulted in the most potent inhibition against c-MET and the highest LipE values observed within this specific series (enzymatic LipE = 4.80 and cell LipE = 4.60) as illustrated in Figure 6. Of note, these are racemates, and the relative potencies of enantiomers will be discussed later. Accordingly, the phenyl substitution pattern of **14k** was the focus for further lead optimization of the 2-aminopyridine series, which next focused

on 5-position derivation to address remaining drug design goals.

Optimization at the 5-Position of the 2-Aminopyridine Series to Crizotinib. With the potent c-MET inhibitor **14k** in hand, design strategies focused on ensuring that potency is maintained while more aggressively tuning physical properties to achieve the ADME profile goals needed for a clinical candidate. Across series, both inhibition data and solved cocrystal structures suggested that substituents extending through the narrow hydrophobic cleft formed by Tyr-1159, Ile-1084, and Gly-1163 into solvent were efficient contributors to potency, provided the necessary planar relationship to the core is maintained. Modeling of 2-aminopyridines suggested that the 5-position vector was the best opportunity to deliver polar groups to the solvent, allowing physical property modulation while optimizing potency. To rapidly test this approach, truncated 2-aminopyridine cores and extended basic amine derivatives from readily available materials were evaluated (Table 2). Expectedly, only modest inhibition was observed for **21**, which has no 5-position substituent. Additionally, **22** and **26** with 5-bromo and 5-cyano groups had similarly weak potency as did the 5-*N*-amide **25**, which introduces polarity too close to the core. Additionally, the 5-phenyl derivative **27** also resulted in micromolar potency. However, greater potency and LipE were achieved with **14k** and **36–38**. A number of factors are potentially contributing to this increase. For these latter compounds, the amide moiety is positioned away from the adenine pocket

Table 2. Structure and Activity Relationship of 5-Substitutes on Racemic 3-(1-(2,6-Dichloro-3-fluorophenyl)ethoxy)pyridin-2-amine


Comp.	R	cLogD ^a	c-MET Ki (μM) ^b	LipE (Ki) ^c	c-MET Cell IC ₅₀ (μM) ^b	LipE (IC ₅₀) ^c
21	H	4.52	7.23	0.62	7.12	0.63
22	Br	6.01	6.56	-0.83	9.92	-1.01
26	CN	4.88	7.58	0.24	>10.0	
25	-NHCOPh	5.30	1.98	0.40	2.90	0.23
27		6.38	1.02	-0.39	1.240	-0.47
14k		3.10	0.012	4.82	0.0203	4.54
36		3.14	0.035	4.32	0.041	4.25
37		2.92	0.075	4.20	0.114	4.02
38		4.48	0.0411	2.91	0.0689	2.68

^a Calculated logarithm of the octanol/water distribution coefficient at pH 7.4 using ACD pchbat, version 9.3. ^b Inhibition constants (K_i)²⁴ and cell IC₅₀^{10a} were determined as described in Experimental Methods. The coefficients of variance were typically less than 20% ($n = 2$). A549 human lung carcinoma cell line was used for the evaluation of the inhibition of autophosphorylation of c-MET. ^c LipE = $\text{p}K_i$ (or pIC_{50}) - cLogD.

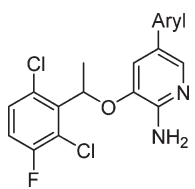
and into solvent, eliminating the desolvation penalty seen for **25**. Furthermore, the amide is electron withdrawing, perhaps contributing to greater planarity arising from conjugation to the amino group of the core and possibly modifying the H-bond donating potential as a result. Last, the solvent exposed basic groups, which lower $\log D$, result in enzymatic and cell LipE values that are at attractive levels, as exemplified with **14k**.

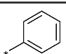
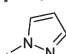
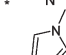
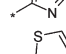
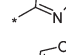
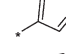
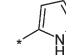
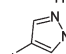
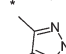
In order to maximize chances of good ADME properties and improved potencies by attenuating torsion strain associated with planar binding, a set of smaller, less lipophilic 5-heteroaryl analogues were prepared as summarized in Table 3. The preference of a five-member heteroaryl group at the 5-position of 2-aminopyridine is consistent with coplanarity of the 5-aryl group with the pyridine scaffold upon binding. The five-member heteroaryl groups also lowered cLogD by about 2 units in general from the phenyl containing **27**. Consequently, compounds **24** and **29–35** showed much improved LipE in the kinase assay, with the weakest improvements coming from compounds **24** and **34**. The performance of **34** is expected because of the methyl groups which destabilize a planar arrangement. To help understand **24**, crystal structures of potent analogues indicate that backbone c-MET protein carbonyl oxygen atoms of residues Met-1160 and Ile-1084 are oriented toward the “ortho” positions of these five-membered

heterocycles. Additional residues at the ligand–protein interface disfavor access of bulk water to these positions, requiring the breaking of solvent H-bonds to the nitrogen lone pair of **24** upon binding. The structural biology, therefore, is consistent with a desolvation penalty and unfavorable electrostatics for compounds such as **24** that present “ortho” electronegative heteroatoms, with capacity as H-bond acceptors only. In contrast, the 5-pyrazol-4-yl group of **33** improved enzymatic and cell potency by 10- to 20-fold, resulting in a cell LipE of 2.83, more than a 3 unit improvement over compound **27**. In this case, the heteroatoms are oriented toward solvent and therefore pay no desolvation penalty. As a result, the pyrazol-4-yl group provided the most potent inhibition against c-MET and the highest LipE value in comparison with other heteroaryl and phenyl groups. Additionally, N-substitution on the pyrazol-4-yl group was well tolerated, as demonstrated by enzymatic and cell potency and an improved cell LipE value of 2.83 for **35**, indicating an attractive design path forward.

For earlier subseries (e.g., **36–38**), extending polar basic groups into solvent was a strategy that consistently improved potency and efficiency. With knowledge that the pyrazole linker provided an extended conformation and vector that resulted in highly efficient cores, a focused lead optimization effort sought to

Table 3. Structure, Activity, and Lipophilicity Relationships of Racemic 5-Aryl Derivatives



Compd.	Aryl	cLogD ^a	c-MET Ki (μM) ^b	LipE (Ki) ^c	c-MET Cell IC ₅₀ (μM) ^b	LipE (IC ₅₀) ^c
27		6.38	1.00	-0.39	1.240	-0.47
24		4.12	3.19	1.38	2.64	1.46
29		4.89	0.24	1.73	1.15	1.05
30		4.60	0.78	1.51	0.74	1.53
31		4.24	0.201	2.45	0.52	2.04
32		4.63	0.348	1.83	0.597	1.59
33		4.68	0.0815	2.41	0.0624	2.52
34		5.60	0.230	1.04	0.333	0.88
35		4.53	0.046	2.80	0.0438	2.83

^a Calculated logarithm of the octanol/water distribution coefficient at pH 7.4 using ACD pchbat, version 9.3. ^b Inhibition constants (K_i)²⁴ and cell IC₅₀^{10a} were determined as described in Experimental Methods. The coefficients of variance were typically less than 20% ($n = 2$). A549 human lung carcinoma cell line was used for the evaluation of the inhibition of autophosphorylation of c-MET. ^c LipE = $\text{p}K_i$ (or pIC_{50}) - cLogD.

combine these structural features to achieve both the potency and the pharmaceutical properties being sought. For polar N-substituents on the pyrazol-4-yl ring, the smallest groups were targeted to provide desirable properties. A set of representative examples are summarized in Table 4.

Overall, N-substituents on the pyrazol-4-yl group maintained or enhanced c-MET inhibition potency while lowering cLogD by almost 3 full units in some cases. Consequently, the introduced structural features improved LipE along with targeted pharmaceutical properties dramatically. The c-MET cell potency vs cLogD data from this and earlier subseries, all 5-aryl derivatives of the 3-(1-(2,6-dichloro-3-fluorophenyl)ethoxy)pyridin-2-amine core, are plotted in Figure 7 to graphically illustrate different efficiency zones with constant LipE values. The data points colored blue represent the 5-pyrazol-4-yl subseries which generally occupied higher LipE space over 5-phenyl subseries (red color). Movement up and to the left, crossing LipE lines, was analyzed for structural features that crossed zones and served as the design goal during optimization. Table 4 indicates that **61**, a racemic version of crizotinib, is one of the most efficient inhibitors, with a c-MET cell IC₅₀ of 0.018 μM and a LipE of 5.62. This is also clear from the plot of all 5-aryl derivatives shown in Figure 7.

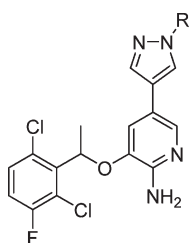
It is important to note that the prototype 5-aryl subseries suffered high metabolic clearance due, in large part, to the high

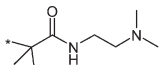
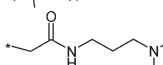
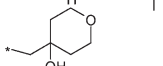
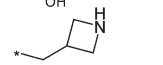
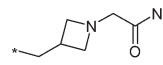
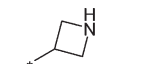
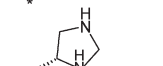
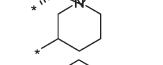
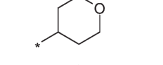
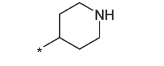
lipophilicity of the key 3-(1-(2,6-dichloro-3-fluorophenyl)ethoxy) group on this novel 2-aminopyridine scaffold. Navigating the results across series, using plots such as Figure 7, facilitates drug design for improved LipE, where metabolic stability improvements are achieved in parallel as summarized in Table 4. Compounds with moderate to stable human metabolic stability were achieved as exemplified by **48** and **61**. With overall good pharmaceutical properties, **61** was chosen for further evaluation.

Compounds in the tables are racemates. The two pure enantiomeric forms of **61** were prepared to evaluate the relative c-MET activity (Figure 8). The *R* enantiomer **63** is significantly more potent, consistent with specific binding as later revealed in a cocrystal structure of crizotinib bound to c-MET (PDB code 2wgi).

The cocrystal structure of crizotinib bound to the nonphosphorylated state of the c-MET kinase domain shows that, as with **3**, the compound binds to an autoinhibitory kinase conformation in which a portion of the kinase activation loop makes direct interactions with the inhibitor (Figure 9). The potency of crizotinib in cells, as was discussed for predecessors **14f** and **14k**, results from key interactions between the α -methylbenzyl unit and the unique c-MET A-loop conformation. The halogenated phenyl group of crizotinib takes a direct and favorable path to form a π - π interaction with Tyr-1230, also

Table 4. Structure, Activity, and Property Relationships of N-Substituents on the 5-Pyrazol-4-yl Ring



Compd	R	c-MET	c-MET Cell	cLog D ^a	LipE (IC ₅₀) ^c	HLM % Remaining ^d
		K _i (μM) ^b	IC ₅₀ (μM) ^b			
35	-CH ₃	0.046	0.0438	4.53	2.83	5.2
44	-CH(CH ₃) ₂	0.0371	0.0356	4.09	2.04	3.2
45		0.0597	0.0653	3.39	3.80	3.60
46		0.0486	0.0760	2.02	5.10	23.8
47		0.0457	0.0406	4.16	3.23	0.9
48		0.0702	0.0453	1.28	6.06	71
49		0.0237	0.0526	2.82	4.46	47.8
50		0.0352	0.0587	1.77	5.56	44.0
58		0.0262	0.0438	2.01	5.35	ND
59		0.014	0.025	2.29	5.31	44.3
60		0.0383	0.0398	4.69	2.71	ND
61		0.0193	0.0183	2.12	5.62	44.6

^a Calculated logarithm of the octanol/water distribution coefficient at pH 7.4 using ACD pchbat, version 9.3. ^b Inhibition constants (K_i)²⁴ and cell IC₅₀^{10a} were determined as described in Experimental Methods. The coefficients of variance were typically less than 20% ($n = 2$). A549 human lung carcinoma cell line was used for the evaluation of the inhibition of autophosphorylation of c-MET. ^c LipE = pK_i (or pIC_{50}) - cLogD. ^d Human liver microsome percent remaining was determined as described in Experimental Methods. ND = not determined.

achieving better distances and aligned geometry between the aryl groups for stacking compared to the case of **3**. Another consequence of the more compact linker of crizotinib is noted when comparing cocrystal structures (Figure 10). The plane of the novel 2-aminopyridine core in crizotinib binds to the hinge in a position that is more consistent with the oxindole in the 1/FGFR1K complex and different from the oxindole in 3/c-MET complex, which was noted earlier to be tilted at approximately a 15° angle. This observation is consistent with less conformational strain associated with binding the more compact 3-benzyloxy-2-aminopyridine compared to **3**. Met-1211 has closer interactions with the phenyl group and 2-aminopyridine core via hydrophobic interactions. Both the 2-chloro and 3-fluoro elements on the 3-benzyloxy group in crizotinib point toward the N-H of Asp-1222, indicating that there may be beneficial electrostatic interactions that replace the sulfonyl oxygen H-bond in **3**. According to the SAR, the α -methyl

and 2,6-dichloro moieties on the 3-benzyloxy group in crizotinib are critical for establishing the low nanomolar cell potency against c-MET. The α -methyl group not only rigidifies the benzyl group but also makes favorable hydrophobic interactions in the pocket surrounded by side chains of residues Val-1092, Leu-1157, Lys-1110, and Ala-1108. As the data and cocrystal structure demonstrate, only the *R*-configuration of the α -methyl group provides the right fit in this lipophilic pocket.

On the other side, the 5-pyrazol-4-yl group is bound through the narrow lipophilic tunnel surrounded by Ile-1084 and Tyr-1159. The terminal piperidine ring, attached to the N1 position of the pyrazol-4-yl, reaches out into the solvent. The cocrystal structure of crizotinib with c-MET confirmed the original design hypotheses, sharing a similar binding mode to **3**. However, crizotinib binds the c-MET kinase domain more efficiently than **3**, resulting in much improved cell-based ligand efficacy (LE) and

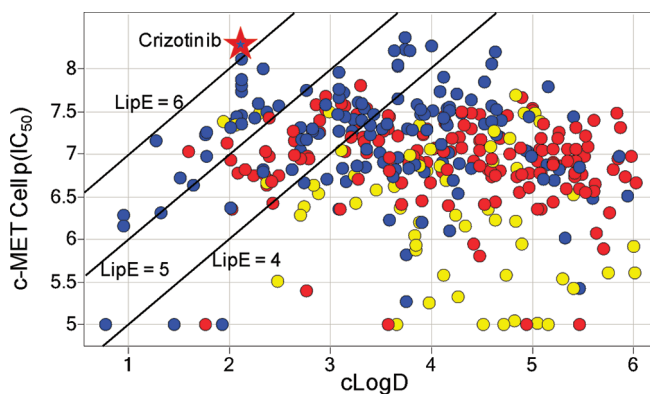


Figure 7. c-MET cell p(IC_{50}) vs cLogD (blue for 5-pyrazol-4-yl, red for 5-phenyl, and yellow for other).

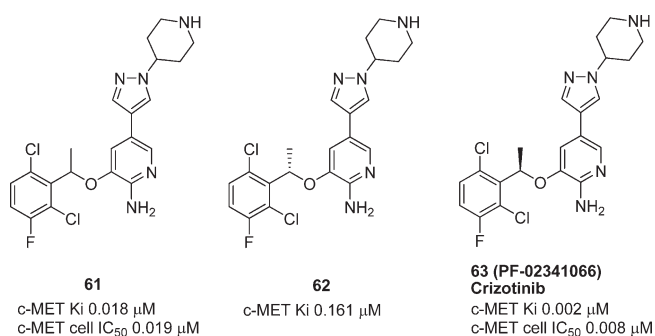


Figure 8. Structure and activity of pure enantiomers of **61**.

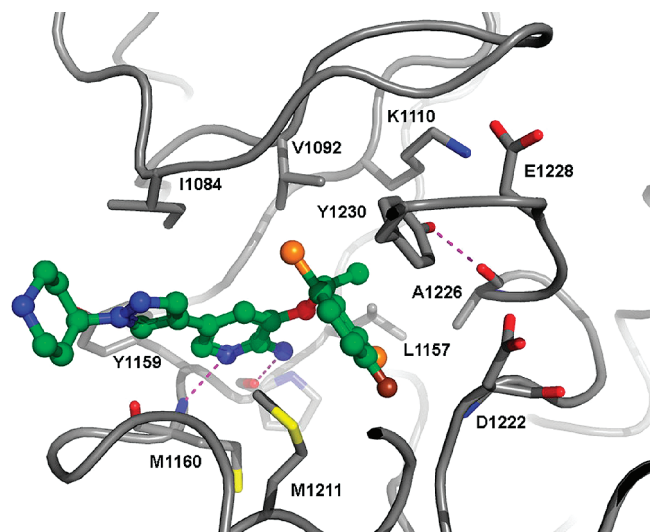


Figure 9. Cocystal structure of crizotinib bound to c-MET.

lipophilic efficiency (LipE) ($LE = 0.379$ and $LipE = 6.14$ for crizotinib; $LE = 0.264$ and $LipE = 4.81$ for **3**).

Kinase Selectivity Profile of Crizotinib. To investigate kinase selectivity, crizotinib was evaluated against a panel of more than 120 human kinases from Upstate Inc. Of these, 13 kinases were inhibited with enzymatic potency within a 100-fold selectivity window of crizotinib enzymatic c-MET potency. To fully account for the unique binding mode accessed by crizotinib, cell-based autophosphorylation assays were employed to determine a

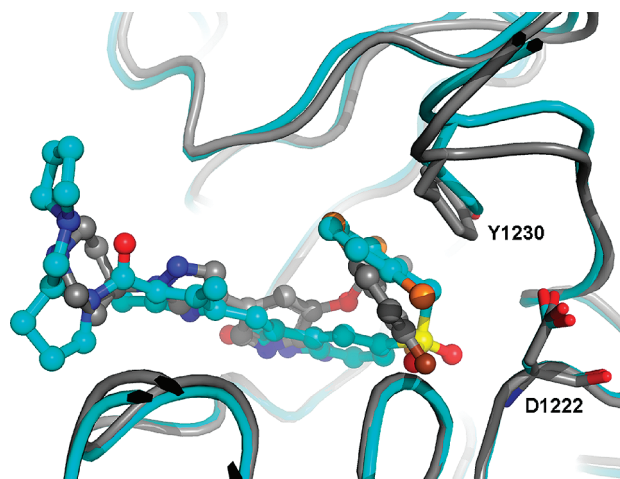


Figure 10. Overlay of crizotinib and **3** bound to c-MET.

more accurate picture of kinase selectivity in the whole cell context. Compared with c-MET cell potency, crizotinib was found to be greater than 1000-fold selective against VEGFR2 and PDGFR β split-RTKs (cell $IC_{50} > 10 \mu$ M), with other cell potency results within the 10μ M limit summarized in Table 5. Selectivity is greater than 200-fold for IR and LCK and approximately 40- to 60-fold for AXL, TIE2, TRKA, and TRKB. Crizotinib selectivity is 10-fold for the c-MET subfamily member RON, which shares 63% sequence identity in the KD and many biological functions with c-MET.²⁶ RON receptor tyrosine kinase is overexpressed and activated in many cancers including breast, colon, and lung and plays important roles in tumor invasive growth and metastasis.²⁷ RON overexpression or coexpression with c-MET correlates with a poor disease free survival in breast, bladder, and gastroesophageal cancers.²⁸ RON is an attractive molecular target for cancer therapy. Furthermore, crizotinib demonstrated a potent cell IC_{50} of 20 nM against an oncogenic ALK kinase fusion protein, NPM-ALK, in a human lymphoma cell line even though ALK shares only 36% kinase domain sequence identity with c-MET. Similar to BCR-ABL in CML, available literature indicates that ALK fusion proteins are also key disease drivers of anaplastic large cell lymphoma, inflammatory myofibroblastic tumor, and non-small cell lung cancer.^{7,29}

In summary, 13 different kinases were inhibited within a 100-fold multiple of c-MET in enzymatic assays. With cellular assays, crizotinib demonstrated potent inhibition of c-MET/ALK, with a 10-fold selectivity window for RON. The high selectivity of crizotinib at the cellular level is related to the unusual binding pocket created by the unique activation loop conformation of nonphosphorylated c-MET as discussed previously. A cocystal structure of ALK kinase domain complexed with crizotinib (PDB code 2xp2) reveals a conformation similar to crizotinib bound to c-MET. The A-loop of ALK shows a notable difference, lacking a π -stacking interaction observed between c-MET Tyr-1230 and crizotinib. The loss of this protein–crizotinib interaction may partially explain the weaker potency observed with ALK. The importance of Tyr-1230–crizotinib interaction in c-MET is further confirmed with Y1230C mutation of c-MET protein, where crizotinib is 10-fold less potent.²⁴ These results are consistent with the weaker potency for crizotinib inhibition of RON kinase, which has a leucine residue at the position of c-MET Tyr-1230. One common interaction among these kinases

Table 5. Kinase Selectivity of Crizotinib

parameter	kinase									
	c-MET	ALK	RON	AXL	TIE2	TRKA	TRKB	ABL	IR	LCK
% inhib (1 μ M) ^a	97.0	99.0	97.0	93.0	97.0	99.3	99.7	91.5	67.7	96.5
enzyme IC ₅₀ (nM) ^a	<1.0	<1.0	NA	<1.0	5.0	<1.0	2.0	24	102	<1.0
cell IC ₅₀ (nM) ^b	8.0	20	80	294	448	580	399	1159	2887	2741

^aData were obtained from Upstate kinase selectivity screens. ^bValues are the average of at least two experiments based on the inhibition of autophosphorylation of targets in the corresponding cell lines with <20% variance.^{10a}

is that of the Met-1211 residue in c-MET. It stabilizes the 2-aminopyridine core, the 3-benzyloxy group, and anchors the scaffold in an L-shape. These important hydrophobic interactions should be retained for RON because of the presence of a methionine residue at the same position. A leucine residue in ALK kinase at the Met-1211 position of c-MET provides similar hydrophobic interactions with crizotinib. Moreover, the high kinase selectivity profile of crizotinib is consistent with pharmacology stemming from a limited set of kinases with potential clinic utility and provides mechanism-based guidance for the expansion of crizotinib to specific additional cancer patient populations.

CHEMISTRY

Compounds **7**, **8**, and **11** were synthesized according to the procedures outlined in Scheme 1. **4** was prepared according to the literature procedures.³⁰ Selective alkylation of the 3-hydroxyl group was achieved under basic conditions by treating with 1 equiv of benzyl bromide and 1 equiv of Cs₂CO₃ in DMF at 80 °C for 4 h to give **6**. Conventional Suzuki coupling conditions provided **7** and **11**. Compound **8** was synthesized via alkylation of **7**.

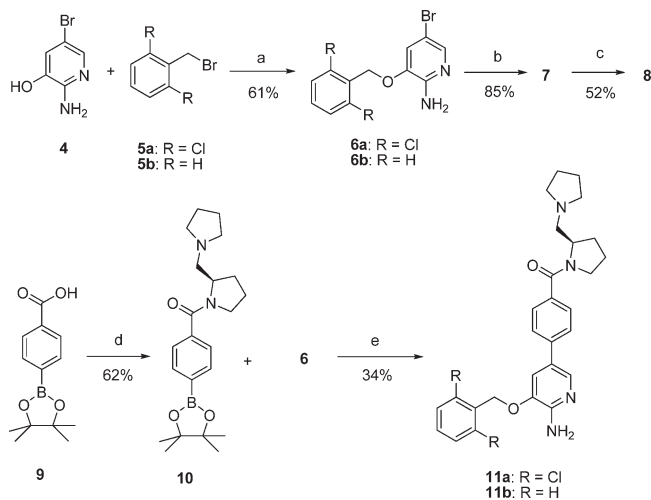
For rapid optimization of substituted 3-benzyloxy groups, compounds were synthesized for evaluation as outlined in Scheme 2. **11b** was prepared according to the procedure described in Scheme 1. After hydrogenolysis, **12** was obtained in a quantitative yield and used to couple with **13** to generate compounds **14a–k**.

Compounds **22** and **23** were prepared according to the procedures in Scheme 3, in order to access a diversity of 5-substituted analogues to support the optimization efforts. Mitsunobu reaction of **16** with **18** provided **20** in high yield, which was further reduced with iron chips in acetic acid and ethanol under reflux to **21**. Bromination and iodination of **21** produced **22** and **23**. A variety of aryl groups were introduced at the 5-position via a Suzuki coupling reaction to provide **27–35**. Compounds **24** and **25** were prepared via copper-catalyzed amination reaction under microwave conditions. The cyano group was introduced under palladium-catalyzed condition to give **26**. Compounds **36–38** were prepared with the conventional amide coupling conditions.

A variety of N-substituted pyrazole analogues were prepared as shown in Scheme 4 via the pyrazole boronic ester **39** or 4-bromopyrazole **41** which was transferred to boronic ester **43** under conventional palladium coupling conditions. Suzuki coupling reaction generated compounds **44–50**. **52** was prepared with oxosulfonium ylide which was generated in situ from trimethylsulfoxonium iodide using NaH in DMSO solvent and coupled with **39** to generate compound **53**.³¹

An alternative route to access N-substituted pyrazole analogues is outlined in Scheme 5. 2-Amino function was protected as a bis-*tert*-butyl carbamate **54** for the preparation of boronic ester **56** with high yield. Acid deprotection of **56** produced **57** which was coupled with **42** to produce compounds **58–61**.

Scheme 1^a

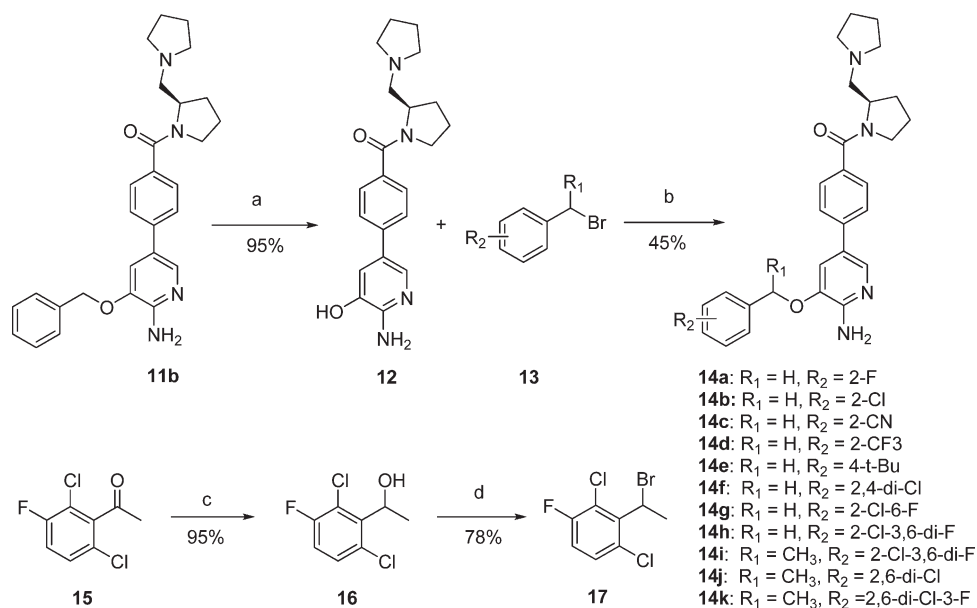


^a Reagents and conditions: (a) Cs₂CO₃, DMF, 80 °C, 4 h; (b) arylboronic ester, Pd(PPh₃)₂Cl₂, Na₂CO₃, DME/H₂O, 80 °C, 12 h; (c) 4-(2-chloroethyl)morpholine, Cs₂CO₃, DMF, 80 °C, 4 h; (d) (R)-1-(pyrrolidin-2-ylmethyl)pyrrolidine, HOBT, EDC, DMF, 1 h; (e) Pd-(dppf)Cl₂, Cs₂CO₃, DME/H₂O, 80 °C, 12 h.

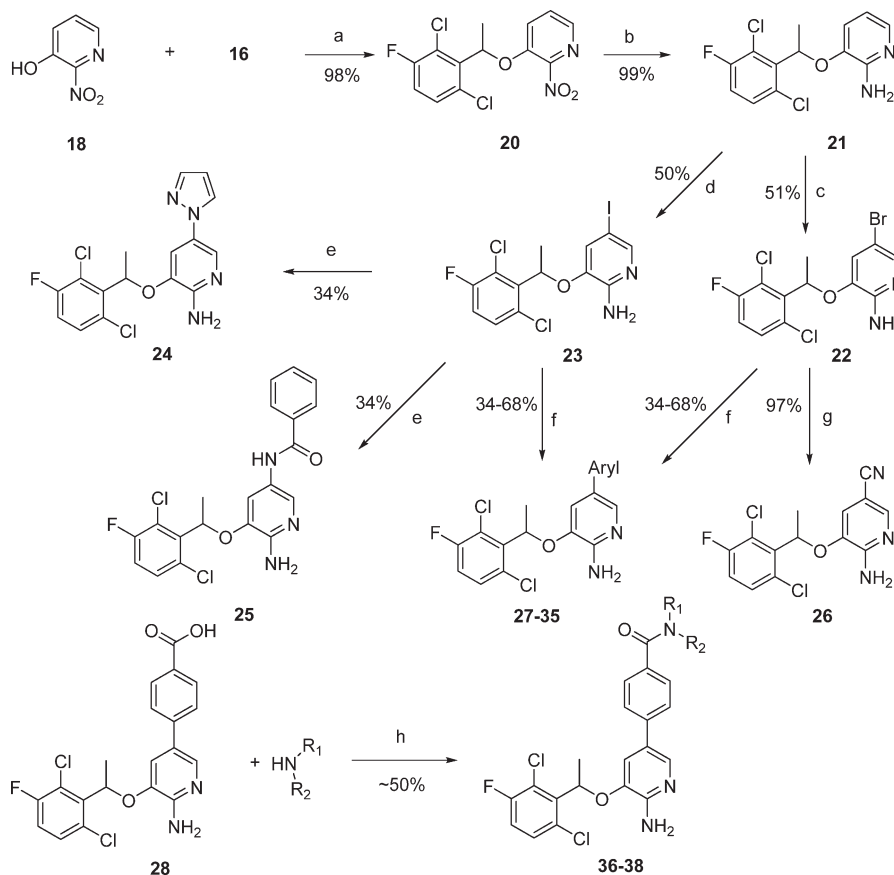
A total synthesis of crizotinib is outlined in Scheme 6. Boronic ester **68** was prepared via alkylation of **66** with piperidinyll derivative **65** followed by palladium coupling with **55**. **69** was prepared with the same synthetic route as the racemic analogue **22** as shown in Scheme 3. (S)-1-(2,6-Dichloro-3-fluorophenyl)ethanol was obtained via a biotransformation method.³² Mitsunobu reaction of (S)-1-(2,6-dichloro-3-fluorophenyl)ethanol with **18** provided (R)-3-(1-(2,6-dichloro-3-fluorophenyl)ethoxy)-2-nitropyridine with >99.5% ee. Suzuki coupling reaction of **69** with **68** followed by deprotection with HCl generated crizotinib in good yield.

CONCLUSIONS

The cocrystal structure of **3**/c-MET complex revealed a novel binding mode of c-MET, which was used to design the novel 5-aryl-3-benzyloxy-2-aminopyridine series. First iteration 5-aryl-3-benzyloxy-2-aminopyridines were moderate c-MET inhibitors. The series was optimized to a highly potent and selective c-MET/ALK dual inhibitor, with a narrower window of selectivity to RON kinase. As shown in Figure 7, LipE and structure based drug design led to crizotinib, which has the highest LipE value. Crizotinib potently inhibited c-MET phosphorylation and c-MET-dependent proliferation, migration, and invasion of human tumor cells in vitro (IC₅₀ of 5–20 nM).^{10a} In addition, crizotinib potently inhibited HGF-stimulated endothelial cell

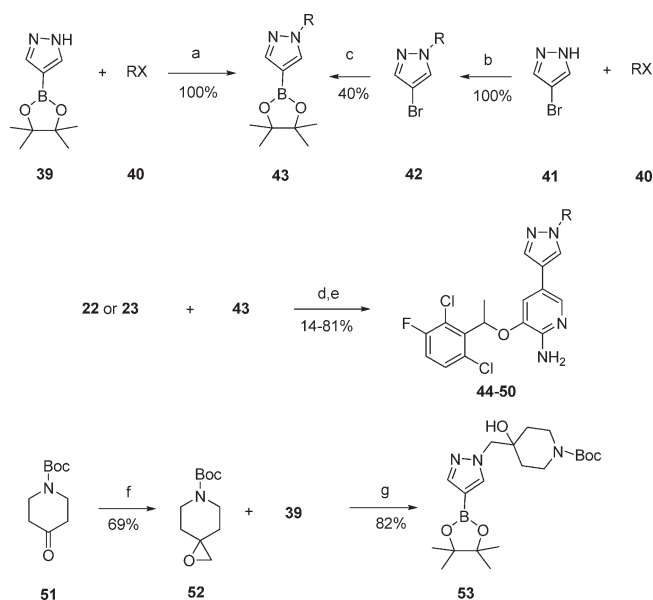
Scheme 2^a

^a Reagents and conditions: (a) H₂ balloon, 10% Pd/C, methanol, 16 h; (b) NaH, DMF, 0 °C to ambient temperature, 2 h; (c) LiAlH₄, THF, 0 °C to ambient temperature, 3 h; (d) Ph₃PBr₂, CH₂Cl₂.

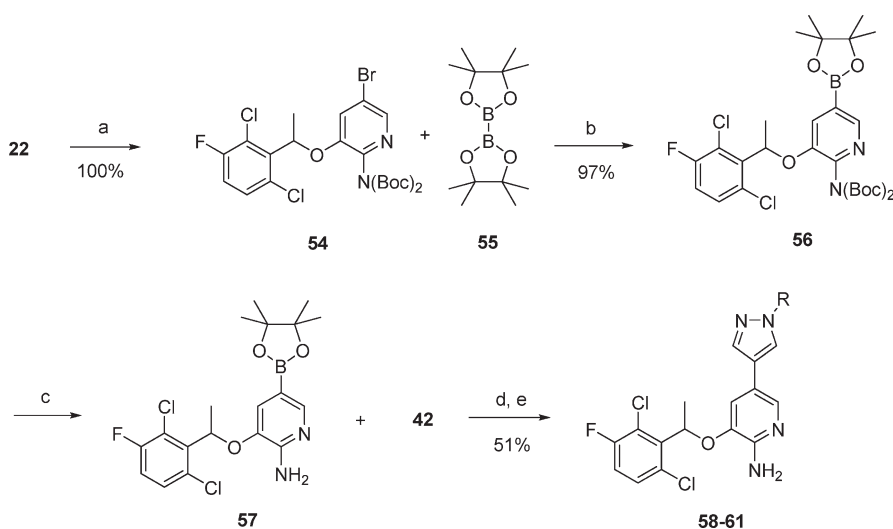
Scheme 3^a

^a Reagents and conditions: (a) Ph₃P, DEAD, THF, 0 °C, 4 h; (b) Fe, AcOH/EtOH, reflux, 1 h; (c) NBS, ACN, 0 °C, 15 min; (d) NIS, ACN/AcOH, 0 °C, 4 h; (e) CuI, K₃PO₄, dodecane/cyclohexanediamine, DMSO, microwave at 150 °C, 2 h; (f) Pd(dppf)Cl₂, Cs₂CO₃, DME/H₂O, 80 °C, 12 h; (g) Zn(CN)₂, Pd₂(dba)₃, DPPF, DMF, 100 °C, 3 h; (h) EDC, HOBt, DMF, 4 h.

survival and invasion and serum-stimulated tubulogenesis *in vitro*, suggesting that this agent also exhibits antiangiogenic properties.^{10a} Crizotinib showed efficacy at well-tolerated doses, including marked cytoreductive antitumor activity, in several tumor models that expressed activated c-MET.^{10a} In biochemical and cellular screens, crizotinib was shown to be selective for c-MET and ALK at pharmacologically relevant concentrations across a panel of >120 diverse kinases. Crizotinib demonstrated tumor cell growth inhibitory activity against cell lines harboring fusion variants or activating mutations of ALK including Karpas 299

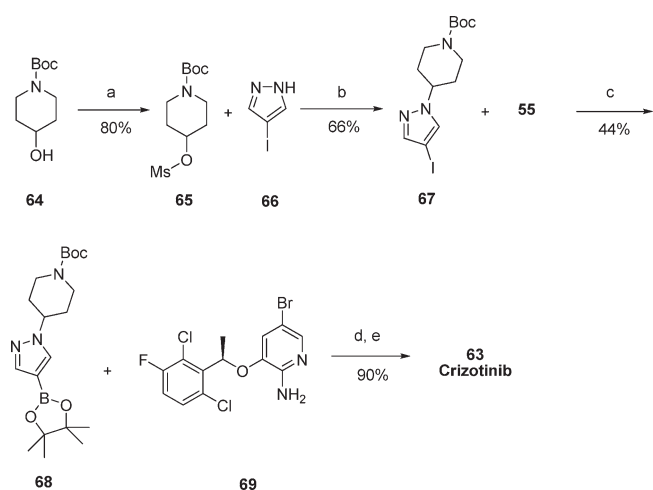
Scheme 4^a

^a Reagents and conditions: (a) Cs₂CO₃, DMF, 90 °C, 12–16 h; (b) NaH, DMF, microwave at 110 °C, 30 min; (c) Pd(dppf)Cl₂, KOAc, DMSO, 80 °C, overnight; (d) Pd(dppf)Cl₂ or Pd(Ph₃P)₂Cl₂, CsF, DME/H₂O, microwave at 120 °C, 1 h; (e) Pd(Ph₃P)₂Cl₂, Na₂CO₃, DME/H₂O, 85 °C, overnight; (f) trimethylsulfoxonium iodide, NaH, DMSO, 55 °C, 6 h; (g) NaH, DMF, 90 °C, 3 h.

Scheme 5^a

^a Reagents and conditions: (a) (Boc)₂O, DMAP, DMF, ambient temperature, 18 h; (b) Pd(dppf)Cl₂, KOAc, DMSO, 80 °C, overnight; (c) 4 N HCl in dioxane, CH₂Cl₂, 40 °C, 12 h; (d) Pd(Ph₃P)₂Cl₂, Na₂CO₃, DME/H₂O, 87 °C, 16 h; (e) 4 N HCl in dioxane, MeOH, 1 h.

(NPM-ALK), SU-DHL-1 (NPM-ALK), Kelly neuroblastoma (activating mutation), and NCI-H3122 (EML4-ALK variant 1) with IC₅₀ values ranging from 74 to 566 nM.¹¹ Crizotinib potently inhibited cell proliferation, which was associated with G₁-S phase cell cycle arrest and induction of apoptosis in ALK-positive ALCL cells (IC₅₀ ≈ 30 nM) but not ALK-negative lymphoma cells.^{10b} Oral administration of crizotinib to severe combined immunodeficient beige mice bearing Karpas 299 ALCL tumor xenografts resulted in dose-dependent antitumor efficacy with complete regression of all tumors at the 100 (mg/kg)/day dose within 15 days of initial compound administration.^{10b} A strong correlation was observed between antitumor response and inhibition of NPM-ALK phosphorylation and induction of apoptosis in tumor tissue.^{10b} Crizotinib demonstrates desirable oral pharmacokinetics in preclinical species, consistent with target modulation and

Scheme 6. Total Synthesis of Crizotinib^a

^a Reagents and conditions: (a) MsCl, Et₃N, CH₂Cl₂; (b) NaH, DMF, 100 °C, overnight; (c) Pd(Ph₃P)₂Cl₂, KOAc, DMSO, 80 °C, 2 h; (d) Pd(dppf)Cl₂, Cs₂CO₃, DME/H₂O, 90 °C, 3 h; (e) 4 N HCl in dioxane, CH₂Cl₂, 0 °C, 4 h.

efficacy, with acceptable pharmacokinetics in patients while being well tolerated.^{33,34} Crizotinib has advanced to human clinical trials and demonstrated remarkable efficacy for patients with non-small-cell lung cancer, inflammatory myofibroblastic tumor, and large cell anaplastic lymphoma harboring fusion ALK genes.³⁵ Early clinical efficacy was also observed for patients with lung, glioblastoma, and esophagogastric adenocarcinoma with c-MET gene amplification.³⁶

EXPERIMENTAL METHODS

General Methods for Chemistry. All reagents and solvents were used as purchased from commercial sources. Reactions were carried out under nitrogen atmosphere unless otherwise indicated. Silica gel chromatography was done using the appropriate size Biotage prepac silica filled cartridges. NMR spectra were generated on a Bruker 300 or 400 MHz instrument and obtained as CDCl₃ or DMSO-*d*₆ solutions (reported in ppm), using CDCl₃ as the reference standard (7.27 ppm) or DMSO-*d*₆ (2.50 ppm). Multiplicities were given as s (singlet), b s (broad singlet), d (doublet), t (triplet), dt (double of triplets), and m (multiplet). Mass spectral data (APCI) were gathered on an Agilent 1100 LC with MSD (Agilent model G1946B upgraded to D model) single-quadrupole mass spec detectors running with atmospheric pressure chemical ionization source. The LC instrument includes a binary pump (Agilent model G1312A) with upper pressure limit of 400 bar attached to an autosampler (Agilent model G1313A) that uses an external tray for sample submission. The column compartment (Agilent model G1316A) is attached to a diode array (Agilent model G1315A). The instrument acquisition and data handling were done with ChemStation, revision B.02.01. The purity measurements were done by measuring peak area at 254 and 224 nm and total ion chromatogram. To evaluate the purity of each peak, UV-vis spectrum from 190 to 700 nm at step size of 2 nm and mass spectrum scan from 150 to 850 amu with cycle time of 0.29 cycle/sec were performed. Retention times (*t*_R) were in minutes, and purity was calculated as percentage of total area. Two HPLC methods were utilized for purity. Method A consisted of the following: Waters Acquity UPLC BEH C18 column, 1.7 μm, 2.1 mm × 100 mm, column temperature 80 °C; solvent A consisting of water (0.1% formic acid and 0.05% ammonium formate); solvent B consisting of methanol (0.1% formic acid and 0.05% ammonium formate); gradient of 5–95% B in 10 min, 95% B in 10–12 min; flow rate of 0.6 mL/min. Method B consisted of the following: EclipseXDB C8 column, 3.5 μm, 4.6 mm × 50 mm, column temperature 40 °C; solvent A consisting of water (5% ACN, 2 mM ammonium acetate, 0.1% acetic acid); solvent B consisting of ACN (5% H₂O, 2 mM ammonium acetate, 0.1% acetic acid); gradient of 20–85% B (0.0–2.5 min), 85–95% B (2.5–3.5 min), 95% B (5 min); flow rate of 0.8 mL/min. Compound purity was determined by combustion analysis (Atlantic Microlabs, Inc.) or high pressure liquid chromatography (HPLC) with a confirming purity of ≥95% for all of the final biological testing compounds.

3-(2,6-Dichlorobenzyloxy)-5-bromopyridin-2-amine (6a). To a solution of 2-amino-5-bromopyridin-3-ol (1.000 g, 5.29 mmol) and 2-(bromomethyl)-1,3-dichlorobenzene (1.270 g, 5.29 mmol) in DMF (20 mL) was added Cs₂CO₃ (1.720 g, 5.29 mmol). The reaction mixture was stirred at 80 °C in an oil bath for 4 h, and LCMS showed the completion of the reaction. The mixture was cooled to ambient temperature, diluted with EtOAc (100 mL), washed with water (30 mL × 5) and brine, and dried over Na₂SO₄. After filtration and condensation, the residue was purified with a silica gel column, eluting with EtOAc/heptane (0–50%) to provide **6a** as an off-white solid (1.120 g, 60.8%): LCMS *m/z* 347 (62%), 349 (100%), 351 (45%) (M + H)⁺; ¹H NMR (400 MHz, DMSO-*d*₆) δ ppm 7.62 (d, *J* = 2.02 Hz, 1H), 7.52–7.59 (m, 2H), 7.44–7.50 (m, 2H), 5.79 (s, 2H), 5.24 (s, 2H). Anal. Calcd for

C₁₂H₄BrCl₂N₂O: C, 41.41; H, 2.61; N, 8.05. Found: C, 41.50; H, 2.51; N, 8.05.

4-(5-(2,6-Dichlorobenzyloxy)-6-aminopyridin-3-yl)phenol (7). A mixture of 3-(2,6-dichlorobenzyloxy)-5-bromopyridin-2-amine (100 mg, 0.29 mmol), 4-(4,4,5,5-tetramethyl-1,3,2-dioxaborolan-2-yl)phenol (86 mg, 0.35 mmol), bis(triphenylphosphine)palladium(II) chloride (8 mg, 0.009 mmol), and sodium carbonate (91 mg, 0.87 mmol) in ethylene glycol dimethyl ether (10 mL) and water (0.5 mL) was degassed and charged with nitrogen three times and then heated in a 80 °C oil bath under nitrogen for 12 h. The mixture was cooled to ambient temperature and diluted with ethyl acetate. The mixture was washed with water, brine and dried over Na₂SO₄. After filtration and condensation, the residue was purified on a silica column, eluting with EtOAc/hexane (0–50%) to afford **7** as a light pink solid (89 mg, 85% yield): LCMS *m/z* 361 (100%), 363 (64%) (M + H)⁺; ¹H NMR (400 MHz, DMSO-*d*₆) δ ppm 9.39 (s, 1H), 7.80 (d, *J* = 1.77 Hz, 1H), 7.53–7.61 (m, 2H), 7.40–7.52 (m, 4H), 6.81 (d, *J* = 8.59 Hz, 2H), 5.52 (s, 2H), 5.33 (s, 2H). HPLC purity (method A): *t*_R = 8.697, 100%.

3-(2,6-Dichlorobenzyloxy)-5-(4-(2-morpholinoethoxy)phenyl)pyridin-2-amine (8). To a solution of **7** (100 mg, 0.247 mmol) and 4-(2-chloroethyl)morpholine (37 mg, 0.247 mmol) in DMF (5 mL) was added Cs₂CO₃ (81 mg, 0.247 mmol). The reaction mixture was heated in a 80 °C oil bath for 4 h. After cooling to ambient temperature, the reaction mixture was filtered and washed with ethyl acetate. The filtrate was condensed and purified on a reversed phase preparative HPLC column, eluting with methanol/water containing 0.1% formic acid. **8** was obtained as a white amorphous solid (61 mg, 52%): LCMS *m/z* 474 (100%), 476 (64%) (M + H)⁺; ¹H NMR (400 MHz, DMSO-*d*₆) δ ppm 7.85 (d, *J* = 1.77 Hz, 1H), 7.53–7.61 (m, 4H), 7.45–7.52 (m, 2H), 7.00 (d, *J* = 8.84 Hz, 2H), 5.59 (s, 2H), 5.35 (s, 2H), 4.09–4.15 (m, 2H), 3.56–3.62 (m, 4H), 2.69–2.75 (m, 2H), 2.46 (m, 4H). HPLC purity (method A): *t*_R = 7.004, 100%.

(R)-(2-(Pyrrolidin-1-ylmethyl)pyrrolidin-1-yl)(4-(4,4,5,5-tetramethyl-1,3,2-dioxaborolan-2-yl)phenyl)methanone (10). To a mixture of 4-(4,4,5,5-tetramethyl-1,3,2-dioxaborolan-2-yl)benzoic acid (**9**, 5.00 g, 20.2 mmol) and (3-(dimethylamino)propyl)ethylcarbodiimide hydrochloride (EDC, 4.88 g, 24.2 mmol) in DMF (100 mL) was added 1,2,3-benzotriazol-1-ol monohydrate (HOBt, 3.57 g, 22.2 mmol). A clear solution was observed after stirring for 30 min, and (R)-1-(pyrrolidin-2-ylmethyl)pyrrolidine (6.22 g, 40.3 mmol) was added to the reaction solution, which was stirred at ambient temperature overnight (12 h). The reaction solution was diluted with EtOAc (500 mL), washed with water (100 mL × 4), saturated Na₂CO₃ solution, brine, and dried over Na₂SO₄. After filtration, evaporation, and high vacuum drying, **10** was obtained as a colorless syrup (4.80 g, 62%): LCMS *m/z* 385 (M + H)⁺; ¹H NMR (400 MHz, DMSO-*d*₆) δ ppm 7.70 (d, *J* = 7.83 Hz, 2H), 7.43 (d, *J* = 7.83 Hz, 2H), 4.15–4.31 (m, 1H), 3.34–3.50 (m, 2H), 3.14–3.26 (m, 1H), 2.61–2.70 (m, 1H), 2.41–2.59 (m, 4H), 1.77–1.90 (m, 4H), 1.58–1.74 (m, 4H), 1.29 (s, 12H).

(R)-(4-(5-(2,6-Dichlorobenzyloxy)-6-aminopyridin-3-yl)phenyl)(2-(pyrrolidin-1-ylmethyl)pyrrolidin-1-yl)methanone (11a). To a solution of **6a** (150 mg, 0.43 mmol) and **9** (248 mg, 0.65 mmol) in DME (3 mL) was added the freshly prepared aqueous solution of Cs₂CO₃ (210 mg, 0.65 mmol) in water (1 mL), followed by the addition of 1,1'-bis(diphenylphosphino)ferrocene palladium dichloride (16.1 mg, 0.022 mmol). The reaction flask was degassed and charged with nitrogen three times and then heated in a 80 °C oil bath overnight (15 h). The reaction solution was diluted with EtOAc, washed with water and brine, and dried over Na₂SO₄. After filtration and concentration, the residue was purified on a reverse phase preparative HPLC column, eluting with methanol/H₂O containing 0.1% formic acid (10–90%), and **11a** was obtained as a white amorphous solid (78 mg, 34% yield): LCMS *m/z* 525 (100%), 527 (64%) (M + H)⁺; ¹H NMR (300 MHz, DMSO-*d*₆, 80 °C) δ ppm 7.99 (d, *J* = 1.88 Hz, 1H), 7.64–7.73 (m, 2H), 7.40–7.61 (m, 6H),

5.52 (s, 2H), 5.42 (s, 2H), 4.16–4.27 (m, 1H), 3.43–3.52 (m, 2H), 3.16–3.26 (m, 1H), 2.54–2.66 (m, 2H), 2.24–2.47 (m, 3H), 1.73–2.08 (m, 4H), 1.58–1.71 (m, 4H). HPLC purity (method A): $t_R = 7.463$, 95.7%.

(R)-(4-(5-Benzyloxy-6-aminopyridin-3-yl)phenyl)(2-(pyrrolidin-1-ylmethyl)pyrrolidin-1-yl)methanone (11b). Compound **11b** was prepared by using a similar procedure described for the synthesis of **11a**: LCMS m/z 457 ($M + H$)⁺; ¹H NMR (300 MHz, DMSO-*d*₆, 80 °C) δ ppm 7.88–7.99 (m, 1H), 7.28–7.69 (m, 10H), 5.65 (s, 2H), 5.27 (s, 2H), 4.07–4.32 (m, 1H), 3.38–3.53 (m, 2H), 2.45 (m, 6H), 1.72–2.12 (m, 5H), 1.54–1.71 (m, 3H). HPLC purity (method A): $t_R = 6.419$, 100%.

(R)-(4-(6-Amino-5-hydroxypyridin-3-yl)phenyl)(2-(pyrrolidin-1-ylmethyl)pyrrolidin-1-yl)methanone (12). To a solution of **11b** (2.28 g, 5.00 mmol) in methanol (25 mL) was added 10% Pd/C (100 mg). The mixture was degassed and charged with hydrogen three times and then stirred under hydrogen balloon for overnight. The mixture was filtered through a Celite pad, washed with methanol, and condensed. After high vacuum drying, **12** was obtained as a white solid (1.74 g, 95% yield): LCMS m/z 367 ($M + H$)⁺; ¹H NMR (400 MHz, DMSO-*d*₆) δ ppm 7.79 (s, 1H), 7.54 (m, 3H), 7.46 (m, 2H), 7.14 (s, 1H), 5.68 (s, 2H), 4.22 (m, 1H), 3.45 (m, 2H), 2.66 (m, 1H), 2.52 (m, 4H), 1.96 (m, 2H), 1.84 (m, 3H), 1.64 (m, 4H).

1-(2,6-Dichloro-3-fluorophenyl)ethanol (16). To a solution of 1-(2,6-dichloro-3-fluorophenyl)ethanone (15.00 g, 72 mmol) in anhydrous THF (150 mL) at 0 °C was added lithium aluminum hydride (2.75 g, 72 mmol) slowly. The mixture was stirred at ambient temperature for 3 h and cooled in an ice bath. Water (3 mL) was dropwise added followed by slow addition of 15% NaOH (3 mL). The mixture was stirred at ambient temperature for 30 min. Then 15% NaOH (9 mL) and MgSO₄ were added and the mixture was filtered to remove solids. The solids were washed with THF (50 mL) and the filtrate was concentrated to give **16** (14.8 g, 95% yield) as a yellow oil: ¹H NMR (400 MHz, DMSO-*d*₆) δ ppm 7.42 (m, 1H), 7.32 (m, 1H), 5.42 (m, 2H), 1.45 (d, $J = 6.4$ Hz, 3H).

2-(1-Bromoethyl)-1,3-dichloro-4-fluorobenzene (17). To a solution of **16** (10.00 g, 47.8 mmol) in anhydrous dichloromethane was added dibromotriphenylphosphorane (22.2 g, 52.6 mmol) portionwise at ambient temperature. The mixture was stirred for 16 h and then concentrated and purified by a silica gel column chromatography with 10% EtOAc in heptane to provide **17** as a colorless liquid (10.14 g, 78% yield). ¹H NMR (300 MHz, DMSO-*d*₆) δ ppm 7.41 (m, 2H), 5.90–6.09 (m, 1H), 2.2 (d, $J = 7.16$ Hz, 3H).

(R)-(4-(5-(2-Fluorobenzyloxy)-6-aminopyridin-3-yl)phenyl)(2-(pyrrolidin-1-ylmethyl)pyrrolidin-1-yl)methanone (14a). To a stirred solution of **12** (100 mg, 0.27 mmol) in anhydrous DMF (15 mL) at 0 °C was added sodium hydride (60% dispersion in mineral oil, 11 mg, 0.49 mmol). The mixture was allowed to stir at 0 °C for 30 min followed by the addition of 1-(bromomethyl)-2-fluorobenzene (51 mg, 0.27 mmol). The reaction mixture was stirred at room temperature for 2 h, diluted with EtOAc, and partitioned with H₂O. The aqueous layer was extracted with EtOAc (2 × 25 mL). The organic layers were combined, washed with H₂O (15 mL), brine (15 mL), and dried over MgSO₄. After filtration and concentration, the residue was purified on a reverse phase preparative HPLC column, eluting with methanol/H₂O containing 0.1% formic acid (10–90%), and **14a** was obtained as a white amorphous solid (58 mg, 45% yield): LCMS m/z 475 ($M + H$)⁺; ¹H NMR (300 MHz, DMSO-*d*₆, 80 °C) δ ppm 7.93–7.99 (m, 1H), 7.48–7.68 (m, 6H), 7.37–7.44 (m, 1H), 7.15–7.28 (m, 2H), 5.64 (br s, 2H), 5.29 (s, 2H), 4.32–4.44 (m, 1H), 3.35–3.57 (m, 3H), 2.03–2.25 (m, 2H), 1.56–2.01 (m, 9H), 1.20–1.36 (m, 2H). HPLC purity (method A): $t_R = 6.515$, 95.5%.

Compounds **14b–l** were prepared by using a similar procedure described for the synthesis of **14a**.

(R)-(4-(5-(2-Chlorobenzyloxy)-6-aminopyridin-3-yl)phenyl)(2-(pyrrolidin-1-ylmethyl)pyrrolidin-1-yl)methanone (14b). LCMS m/z 491 ($M + H$)⁺; ¹H NMR (300 MHz, DMSO-*d*₆, 80 °C)

δ ppm 7.95 (d, $J = 1.88$ Hz, 1H), 7.68–7.74 (m, 1H), 7.62–7.66 (m, 2H), 7.45–7.54 (m, 4H), 7.33–7.43 (m, 2H), 5.65 (s, 2H), 5.32 (s, 2H), 4.16–4.25 (m, 1H), 3.42–3.50 (m, 2H), 3.20–3.24 (m, 1H), 2.53–2.61 (m, 2H), 2.37–2.45 (m, 3H), 1.73–2.06 (m, 4H), 1.58–1.68 (m, 4H). HPLC purity (method A): $t_R = 6.812$, 98.7%.

(R)-2-((2-Amino-5-(4-(2-(pyrrolidin-1-ylmethyl)pyrrolidin-1-carbonyl)phenyl)pyridin-3-yloxy)methyl)benzotrile (14c). LCMS m/z 582 ($M + H$)⁺; ¹H NMR (300 MHz, DMSO-*d*₆, 80 °C) δ ppm 7.91–8.00 (m, 2H), 7.81–7.89 (m, 1H), 7.73–7.81 (m, 1H), 7.69 (d, $J = 7.91$ Hz, 2H), 7.48–7.61 (m, 4H), 5.93 (s, 2H), 5.41 (s, 2H), 4.09–4.37 (m, 1H), 3.45–3.52 (m, 4H), 2.55–2.66 (m, 3H), 2.40–2.47 (m, 1H), 1.85–2.02 (m, 4H), 1.57–1.75 (m, 4H). HPLC purity (method A): $t_R = 5.573$, 98.9%.

(R)-(4-(5-(2-Trifluoromethylbenzyloxy)-6-aminopyridin-3-yl)phenyl)(2-(pyrrolidin-1-ylmethyl)pyrrolidin-1-yl)methanone (14d). LCMS m/z 525 ($M + H$)⁺; ¹H NMR (300 MHz, DMSO-*d*₆, 80 °C) δ ppm 7.97 (d, $J = 1.88$ Hz, 1H), 7.88 (d, $J = 7.54$ Hz, 1H), 7.70–7.83 (m, 2H), 7.57–7.66 (m, 3H), 7.51 (d, $J = 8.29$ Hz, 2H), 7.44 (d, $J = 1.88$ Hz, 1H), 5.54–5.81 (m, 2H), 5.39 (s, 2H), 4.15–4.32 (m, 2H), 3.47 (t, $J = 5.75$ Hz, 2H), 2.52–2.67 (m, 3H), 2.30–2.47 (m, 2H), 1.75–2.06 (m, 4H), 1.56–1.75 (m, 4H). HPLC purity (method A): $t_R = 7.400$, 100%.

(R)-(4-(5-(4-tert-Butylbenzyloxy)-6-aminopyridin-3-yl)phenyl)(2-(pyrrolidin-1-ylmethyl)pyrrolidin-1-yl)methanone (14e). LCMS m/z 513 ($M + H$)⁺; ¹H NMR (300 MHz, DMSO-*d*₆, 80 °C) δ ppm 7.92 (d, $J = 1.88$ Hz, 1H), 7.59–7.64 (m, 2H), 7.49 (d, $J = 8.10$ Hz, 2H), 7.39–7.46 (m, 5H), 5.62 (br s, 2H), 5.21 (s, 2H), 4.17–4.29 (m, 1H), 3.39–3.51 (m, 3H), 2.51–2.65 (m, 3H), 2.33–2.47 (m, 2H), 1.75–2.06 (m, 4H), 1.62–1.71 (m, 4H), 1.31 (s, 9H). HPLC purity (method A): $t_R = 8.664$, 96.5%.

(R)-(4-(5-(2,4-Dichlorobenzyloxy)-6-aminopyridin-3-yl)phenyl)(2-(pyrrolidin-1-ylmethyl)pyrrolidin-1-yl)methanone (14f). LCMS m/z 525 (100%), 527 (64%) ($M + H$)⁺; ¹H NMR (300 MHz, DMSO-*d*₆, 80 °C) δ ppm 7.97 (d, $J = 1.88$ Hz, 1H), 7.75 (d, $J = 8.48$ Hz, 1H), 7.60–7.70 (m, 3H), 7.43–7.54 (m, 4H), 5.69 (s, 2H), 5.31 (s, 2H), 4.15–4.29 (m, 1H), 3.41–3.52 (m, 2H), 3.19–3.24 (m, 1H), 2.53–2.61 (m, 2H), 2.34–2.48 (m, 3H), 1.76–2.02 (m, 4H), 1.58–1.69 (m, 4H). HPLC purity (method A): $t_R = 7.987$, 95.95%.

(R)-(4-(5-(2-Chloro-6-fluorobenzyloxy)-6-aminopyridin-3-yl)phenyl)(2-(pyrrolidin-1-ylmethyl)pyrrolidin-1-yl)methanone (14g). LCMS m/z 509 (100%), 510 (32%) ($M + H$)⁺; ¹H NMR (300 MHz, DMSO-*d*₆, 80 °C) δ ppm 7.98 (d, $J = 2.07$ Hz, 1H), 7.62–7.71 (m, 2H), 7.38–7.63 (m, 5H), 7.24–7.36 (m, 1H), 5.53 (s, 2H), 5.34 (d, $J = 1.88$ Hz, 2H), 4.18–4.30 (m, 1H), 3.46–3.51 (m, 2H), 3.20–3.24 (m, 1H), 2.55–2.61 (m, 2H), 2.32–2.48 (m, 3H), 1.76–2.12 (m, 4H), 1.61–1.70 (m, 4H). HPLC purity (method A): $t_R = 6.909$, 100%.

(R)-(4-(5-(2-Chloro-3,6-difluorobenzyloxy)-6-aminopyridin-3-yl)phenyl)(2-(pyrrolidin-1-ylmethyl)pyrrolidin-1-yl)methanone (14h). LCMS m/z 527 (100%), 529 (32%) ($M + H$)⁺; ¹H NMR (300 MHz, DMSO-*d*₆, 80 °C) δ ppm 7.99 (d, $J = 1.88$ Hz, 1H), 7.68 (d, $J = 8.48$ Hz, 2H), 7.46–7.62 (m, 4H), 7.31–7.44 (m, 1H), 5.57 (s, 2H), 5.33–5.39 (m, 2H), 4.19–4.31 (m, 1H), 3.45–3.52 (m, 2H), 3.19–3.26 (m, 1H), 2.54–2.61 (m, 2H), 2.35–2.47 (m, 3H), 1.78–2.09 (m, 4H), 1.59–1.70 (m, 4H). HPLC purity (method A): $t_R = 6.821$, 96.3%.

(4-(6-Amino-5-(1-(2-chloro-3,6-difluorophenyl)ethoxy)pyridin-3-yl)phenyl)((R)-2-(pyrrolidin-1-ylmethyl)pyrrolidin-1-yl)methanone (14i). LCMS m/z 541 (100%), 543 (32%) ($M + H$)⁺; ¹H NMR (300 MHz, DMSO-*d*₆, 80 °C) δ ppm 7.89 (d, $J = 1.88$ Hz, 1H), 7.34–7.60 (m, 5H), 7.22–7.33 (m, 1H), 7.18 (d, $J = 1.88$ Hz, 1H), 5.89–6.08 (m, 1H), 5.61 (s, 2H), 4.01–4.29 (m, 1H), 3.28–3.52 (m, 2H), 2.28–2.48 (m, 6H), 1.67–2.13 (m, 8H), 1.51–1.69 (m, 3H). HPLC purity (method A): $t_R = 7.865$, 100%.

(4-(6-Amino-5-(1-(2,6-dichlorophenyl)ethoxy)pyridin-3-yl)phenyl)((R)-2-(pyrrolidin-1-ylmethyl)pyrrolidin-1-yl)methanone (14j). LCMS m/z 539 (100%), 541 (64%) ($M + H$)⁺. ¹H NMR (300 MHz,

DMSO- d_6 , 80 °C) δ ppm 7.88 (s, 1H), 7.39–7.51 (m, 6H), 7.24–7.39 (m, 1H), 7.05 (s, 1H), 6.06–6.22 (m, 1H), 5.67 (s, 2H), 4.14–4.30 (m, 1H), 3.39–3.50 (m, 2H), 2.30–2.48 (m, 5H), 1.73–2.10 (m, 8H), 1.60–1.71 (m, 4 H). HPLC purity (method A): t_R = 8.329, 100%.

(R)-(4-(6-Amino-5-(1-(2,6-dichloro-3-fluorophenyl)ethoxy)pyridin-3-yl)phenyl)((R)-2-(pyrrolidin-1-ylmethyl)pyrrolidin-1-yl)methanone (14k). LCMS m/z 557 (100%), 559 (64%) (M + H)⁺. ¹H NMR (300 MHz, DMSO- d_6 , 80 °C) δ ppm 7.90 (d, J = 1.51 Hz, 1H), 7.50–7.61 (m, 1H), 7.36–7.49 (m, 5H), 7.06 (d, J = 1.88 Hz, 1H), 6.11–6.23 (m, 1H), 5.70 (s, 2H), 4.13–4.26 (m, 1H), 3.46 (t, J = 6.78 Hz, 2H), 2.32–2.49 (m, 6H), 1.75–2.04 (m, 4H), 1.56–1.70 (m, 4H). HPLC purity (method A): t_R = 8.010, 100%.

3-(1-(2,6-Dichloro-3-fluorophenyl)ethoxy)-2-nitropyridine (20). To a stirred solution of triphenylphosphine (8.2 g, 0.03 mol) and DEAD (13.65 mL of a 40% solution in toluene) in THF (200 mL) at 0 °C was added a solution of 1-(2,6-dichloro-3-fluorophenyl)ethanol (4.55 g, 0.021 mol) and 3-hydroxynitropyridine (3.35 g, 0.023 mol) in THF (200 mL). The resulting bright orange solution was stirred under a nitrogen atmosphere at ambient temperature for 4 h at which point all starting materials had been consumed. The solvent was removed, and the crude material was dry loaded onto a silica gel column and eluted with ethyl acetate–hexanes (20:80) to yield **20** (6.21 g, 0.021 mol, 98%) as an off-white solid: ¹H NMR (400 MHz, DMSO- d_6) δ ppm 8.08 (dd, J = 4.67, 1.14 Hz, 1H), 7.68 (dd, J = 8.59, 4.55 Hz, 1H), 7.53–7.59 (m, 1H), 7.43–7.51 (m, 2H), 6.27 (q, J = 6.74 Hz, 1H), 1.74 (d, J = 6.57 Hz, 3H).

3-(1-(2,6-Dichloro-3-fluorophenyl)ethoxy)pyridin-2-amine (21). To a stirred mixture of AcOH (650 mL) and EtOH (500 mL) were suspended **20** (9.43 g, 0.028 mol) and iron chips (15.7 g, 0.28 mol). The mixture was heated slowly to reflux and allowed to stir for 1 h. The mixture was cooled to room temperature. Then diethyl ether (500 mL) and water (500 mL) were added. The solution was carefully neutralized by the addition of sodium carbonate. The combined organic extracts were washed with saturated NaHCO₃ (2 × 100 mL), H₂O (2 × 100 mL), and brine (1 × 100 mL) and then dried (Na₂SO₄), filtered, and concentrated to dryness under vacuum to yield **21** (9.04 g, 99%) as an off-white solid: LCMS m/z 301 (100%), 303 (64%) (M + H)⁺; ¹H NMR (400 MHz, DMSO- d_6) δ ppm 7.51–7.58 (m, 1H), 7.40–7.50 (m, 2H), 6.62 (dd, J = 7.83, 1.01 Hz, 1H), 6.38 (dd, J = 7.83, 5.05 Hz, 1H), 5.96 (q, J = 6.65 Hz, 1H), 5.66 (s, 2H), 1.76 (d, J = 6.57 Hz, 3H). HPLC purity (method A): t_R = 7.185, 99.3%.

5-Bromo-3-(1-(2,6-dichloro-3-fluorophenyl)ethoxy)pyridin-2-amine (22). A stirring solution of **21** (9.07 g, 0.03 mol) in acetonitrile was cooled to 0 °C using an ice bath. To this solution was added *N*-bromosuccinimide (NBS) (5.33 g, 0.03 mol) portionwise. The mixture was stirred at 0 °C for 15 min. The mixture was concentrated to dryness under vacuum. The resulting dark oil was purified via a silica gel column, eluting with ethyl acetate/hexane (1:5), and **22** was obtained as a white crystalline solid (5.8 g, 51%): LCMS m/z 379 (62%), 381 (100%), 383 (45%) (M + H)⁺; ¹H NMR (400 MHz, DMSO- d_6) δ ppm 7.52–7.62 (m, 2H), 7.43–7.51 (m, 1H), 6.75 (d, J = 1.77 Hz, 1H), 5.94–6.05 (m, 3H), 1.77 (d, J = 6.82 Hz, 3H). Anal. Calcd for C₁₃H₁₀BrCl₂FN₂O: C, 41.09; H, 2.65; N, 7.37. Found: C, 41.20; H, 2.54; N, 7.34.

5-Iodo-3-(1-(2,6-dichloro-3-fluorophenyl)ethoxy)pyridin-2-amine (23). To a solution of **21** (10.0 g, 33.2 mmol) in acetonitrile (600 mL) and acetic acid (120 mL) was added *N*-iodosuccinimide (11.2 g, 49.8 mmol). The mixture was stirred at room temperature for 4 h, and the reaction was quenched with Na₂S₂O₅ solution. After evaporation, the residue was partitioned between ethyl acetate and water. The organic layer was washed with aqueous NaOH solution (2 N), brine and dried over Na₂SO₄. The crude product was purified on a silica gel column, eluting with ethyl acetate/hexane (1:5) to provide **23** as an off-white solid (7.1 g, 50% yield): LCMS m/z 427 (100%), 429 (64%) (M + H)⁺; ¹H NMR (300 MHz, DMSO- d_6) δ ppm 7.63 (d, J = 1.70 Hz, 1H), 7.51–7.60 (m, 1H), 7.37–7.51 (m, 1H), 6.84 (d, J = 1.70 Hz, 1H),

5.82–6.06 (m, 3H), 1.76 (d, J = 6.59 Hz, 3H). Anal. Calcd for C₁₃H₁₀Cl₂FIN₂O: C, 36.56; H, 2.36; N, 6.56. Found: C, 36.85; H, 2.28; N, 6.42.

3-(1-(2,6-Dichloro-3-fluorophenyl)ethoxy)-5-(1H-pyrazol-1-yl)pyridin-2-amine (24). To a stirred solution of **23** (100 mg, 0.23 mmol) and pyrazole (48 mg, 0.70 mmol) in DMSO (1 mL) were added K₃PO₄ (101 mg, 0.47 mmol), dodecane (0.015 mL, 0.05 mmol), cyclohexanediamine (0.009 mL, 0.07 mmol), and copper iodide (CuI) (14 mg, 0.07 mmol). The solution was bubbled with nitrogen for 5 min, then irradiated with microwave at 150 °C for 2 h. The mixture was purified by preparative reverse phase HPLC to produce **24** as an amorphous white solid (38 mg, yield 34%): LCMS m/z 367 (100%), 369 (64%) (M + H)⁺; ¹H NMR (400 MHz, DMSO- d_6) δ ppm 8.21 (d, J = 2.53 Hz, 1H), 7.95 (d, J = 2.02 Hz, 1H), 7.67 (d, J = 1.77 Hz, 1H), 7.57 (dd, J = 8.97, 4.93 Hz, 1H), 7.45 (t, J = 8.72 Hz, 1H), 7.29 (d, J = 1.77 Hz, 1H), 6.46–6.52 (m, 1H), 6.16 (t, J = 6.57 Hz, 1H), 1.81 (d, J = 6.57 Hz, 3H).

N-(6-Amino-5-(1-(2,6-dichloro-3-fluorophenyl)ethoxy)pyridin-3-yl)benzamide (25). Compound **25** was prepared by using a similar procedure described for the synthesis of compound **24**: LCMS m/z 420 (100%), 422 (64%) (M + H)⁺; ¹H NMR (400 MHz, DMSO- d_6) δ ppm 10.31 (s, 1H), 7.93 (s, 1H), 7.83 (d, J = 7.33 Hz, 2H), 7.48–7.60 (m, 5H), 7.37 (d, J = 1.52 Hz, 1H), 6.06 (q, J = 6.57 Hz, 1H), 1.75–1.85 (m, 4H). HPLC purity (method A): t_R = 9.457, 98.0%.

6-Amino-5-(1-(2,6-dichloro-3-fluorophenyl)ethoxy)nicotinonitrile (26). To a solution of **22** (5.00 g, 13.15 mmol) in DMF (73 mL) and water (1 mL) were added Zn(CN)₂ (4.50 g, 26.3 mmol), Pd₂(dba)₃ (0.602 g, 0.65 mmol), and DPPF (0.86 g, 1.55 mmol). The mixture was degassed and charged with nitrogen three times and then stirred under nitrogen at 100 °C for 3 h. The reaction solution was partitioned between ethyl acetate and water. The organic layer was washed with a solution of saturated NH₄Cl–concentrated NH₄OH–water (4:1:4), then dried over MgSO₄. The crude product was purified on a silica gel column, eluting with ethyl acetate–hexanes (1:4) to provide **26** as a white solid (4.15 g, 97% yield): LCMS m/z 326 (100%), 328 (64%) (M + H)⁺; ¹H NMR (400 MHz, DMSO- d_6) δ ppm 7.93 (d, J = 1.77 Hz, 1H), 7.57 (dd, J = 9.09, 5.05 Hz, 1H), 7.46 (t, J = 8.72 Hz, 1H), 6.88 (br s, 2H), 6.75 (d, J = 1.77 Hz, 1H), 6.03 (q, J = 6.57 Hz, 1H), 1.76 (d, J = 6.57 Hz, 3H). HPLC purity (method A): t_R = 9.656, 98.9%.

Compounds **27–35** were prepared according to a similar procedure described for the synthesis of compound **11a**.

3-(1-(2,6-Dichloro-3-fluorophenyl)ethoxy)-5-phenylpyridin-2-amine (27). LCMS m/z 377 (100%), 379 (64%) (M + H)⁺; ¹H NMR (400 MHz, DMSO- d_6) δ ppm 7.82 (d, J = 2.02 Hz, 1H), 7.57 (dd, J = 8.97, 4.93 Hz, 1H), 7.40–7.49 (m, 1H), 7.30–7.40 (m, 4H), 7.25 (ddd, J = 5.18, 3.54, 3.41 Hz, 1H), 6.94 (d, J = 2.02 Hz, 1H), 6.07–6.17 (m, 1 H), 5.88 (s, 2H), 1.81 (d, J = 6.82 Hz, 3H). HPLC purity (method A): t_R = 10.094, 98.4%.

4-(6-Amino-5-(1-(2,6-dichloro-3-fluorophenyl)ethoxy)pyridin-3-yl)benzoic Acid (28). LCMS m/z 421 (100%), 423 (64%) (M + H)⁺; ¹H NMR (400 MHz, DMSO- d_6) δ ppm 7.80–7.91 (m, 3H), 7.59 (dd, J = 9.09, 5.05 Hz, 1H), 7.40–7.50 (m, 1H), 7.36 (d, J = 8.08 Hz, 2H), 6.99 (d, J = 1.77 Hz, 1H), 6.15 (q, J = 6.57 Hz, 1H), 5.92 (s, 2H), 1.82 (d, J = 6.57 Hz, 3H). HPLC purity (method A): t_R = 8.335, 95.5%.

3-(1-(2,6-Dichloro-3-fluorophenyl)ethoxy)-5-(1-methyl-1H-imidazol-4-yl)pyridin-2-amine (29). LCMS m/z 381 (100%), 383 (64%) (M + H)⁺; ¹H NMR (400 MHz, DMSO- d_6) δ ppm 7.30–7.39 (m, 3H), 7.22 (t, J = 8.72 Hz, 1H), 6.51 (s, 1H), 6.40 (d, J = 1.77 Hz, 1H), 5.80 (q, J = 6.65 Hz, 1H), 5.73 (s, 2H), 3.18 (s, 3H), 1.55 (d, J = 6.57 Hz, 3H). Anal. Calcd for C₁₇H₁₅N₄OCl₂F·0.1H₂O: C, 53.31; H, 4.00; N, 14.63. Found: C, 53.28; H, 4.08; N, 14.31.

3-(1-(2,6-Dichloro-3-fluorophenyl)ethoxy)-5-(thiazol-2-yl)pyridin-2-amine (30). LCMS m/z 384 (100%), 386 (64%) (M + H)⁺; ¹H NMR (400 MHz, DMSO- d_6) δ ppm 8.10 (d, J = 1.77 Hz, 1H), 7.76

(d, $J = 3.28$ Hz, 1H), 7.53–7.64 (m, 2H), 7.45 (t, $J = 8.72$ Hz, 1H), 7.12 (d, $J = 1.77$ Hz, 1H), 6.35 (s, 2H), 6.10 (q, $J = 6.48$ Hz, 1H), 1.82 (d, $J = 6.57$ Hz, 3H). HPLC purity (method A): $t_R = 10.417$, 100%.

3-(1-(2,6-Dichloro-3-fluorophenyl)ethoxy)-5-(isoxazol-4-yl)pyridin-2-amine (31). LCMS m/z 368 (100%), 370 (64%) ($M + H$)⁺; ¹H NMR (400 MHz, MeOD) δ ppm 8.68 (s, 1H), 8.50 (s, 1H), 7.64 (s, 1H), 7.36 (dd, $J = 8.97, 4.93$ Hz, 1H), 7.13 (t, $J = 8.72$ Hz, 1H), 6.87 (s, 1H), 6.11 (q, $J = 6.57$ Hz, 1H), 1.78 (d, $J = 6.82$ Hz, 3H). HPLC purity (method A): $t_R = 3.441$, 100%.

3-(1-(2,6-Dichloro-3-fluorophenyl)ethoxy)-5-(1H-pyrazol-5-yl)pyridin-2-amine (32). LCMS m/z 367 (100%), 369 (64%) ($M + H$)⁺; ¹H NMR (400 MHz, DMSO- d_6) δ ppm 7.92 (d, $J = 1.52$ Hz, 1H), 7.68 (s, 1H), 7.49–7.59 (m, 1H), 7.43 (t, $J = 8.72$ Hz, 2H), 7.12 (s, 1H), 6.41 (s, 1H), 6.06 (s, 1H), 5.90 (s, 2H), 3.32 (s, 4H), 1.78 (d, $J = 6.57$ Hz, 3H).

3-(1-(2,6-Dichloro-3-fluorophenyl)ethoxy)-5-(1H-pyrazol-4-yl)pyridin-2-amine (33). Yield: 53.6%. LCMS m/z 367 (100%), 369 (64%) ($M + H$)⁺; ¹H NMR (400 MHz, CDCl₃) δ ppm 7.80 (d, $J = 1.52$ Hz, 1H), 7.67 (s, 2H), 7.22–7.33 (m, 1H), 6.96–7.06 (m, 1H), 6.89 (d, $J = 1.77$ Hz, 1H), 6.06 (q, $J = 6.57$ Hz, 1H), 5.07 (s, 2H), 1.84 (d, $J = 6.57$ Hz, 3H), 1.60 (s, 1H). Anal. Calcd for C₁₆H₁₃N₄OCl₂F·0.5 CH₃OH·0.1CH₂Cl₂: C, 50.90; H, 3.91; N, 14.30. Found: C, 50.60; H, 3.94; N, 14.57.

3-(1-(2,6-Dichloro-3-fluorophenyl)ethoxy)-5-(3,5-dimethyl-1H-pyrazol-4-yl)pyridin-2-amine (34). LCMS m/z 395 (100%), 397 (64%) ($M + H$)⁺; ¹H NMR (400 MHz, CDCl₃) δ ppm 7.36 (dd, $J = 8.84, 4.80$ Hz, 1H), 7.21 (d, $J = 1.26$ Hz, 1H), 7.11–7.19 (m, 1H), 6.71 (s, 1H), 6.05–6.16 (m, 1H), 2.14 (s, 6H), 1.93 (d, $J = 6.57$ Hz, 3H). HPLC purity (method A): $t_R = 8.335$, 100%.

3-(1-(2,6-Dichloro-3-fluorophenyl)ethoxy)-5-(1-methyl-1H-pyrazol-4-yl)pyridin-2-amine (35). Yield: 68.4%. LCMS m/z 381 (100%), 383 (64%) ($M + H$)⁺; ¹H NMR (400 MHz, CDCl₃) δ ppm 7.74 (d, $J = 1.77$ Hz, 1H), 7.53 (s, 1H), 7.40 (s, 1H), 7.28 (dd, $J = 8.97, 4.93$ Hz, 1H), 7.03 (m, 1H), 6.84 (d, $J = 1.77$ Hz, 1H), 6.05 (q, $J = 6.57$ Hz, 1H), 4.76 (s, 2H), 3.89 (s, 3H), 1.84 (d, $J = 6.82$ Hz, 3H). Anal. Calcd for C₁₇H₁₅N₄OCl₂F·0.5H₂O: C, 52.32; H, 4.13; N, 14.36. Found: C, 52.51; H, 4.00; N, 14.30.

General Procedure A for Amide Formation. To a solution of 6-amino-5-(substituted benzyloxy)pyridin-3-yl]benzoic acid (1 mol equiv), 1-hydroxybenzotriazole hydrate (HOBT, 1.2 mol equiv), and 1-(3-dimethylaminopropyl)-3-ethylcarbodiimide hydrochloride (EDC, 1.2 mol equiv) in DMF (0.2 M) was added amine (1.2 mol equiv). The reaction solution was stirred at room temperature overnight, then diluted with EtOAc and partitioned with H₂O. The organic layer was separated, and the aqueous layer was extracted with EtOAc. The combined organic layers were washed with water, saturated NaHCO₃, and brine. The solution was dried over Na₂SO₄, filtered, and concentrated to dryness under vacuum. The residue was purified using column chromatography (silica gel, 99:1 to 95:5 CH₂Cl₂/MeOH). The fractions containing product were concentrated under vacuum to yield the amide product with a yield of ~50%.

Compounds 36–38 were prepared according to general procedure B for amide formation.

(4-(6-Amino-5-(1-(2,6-dichloro-3-fluorophenyl)ethoxy)pyridin-3-yl)phenyl)(4-(pyrrolidin-1-yl)piperidin-1-yl)methanone (36). LCMS m/z 557 (100%), 559 (64%) ($M + H$)⁺; ¹H NMR (400 MHz, DMSO- d_6) δ ppm 7.88 (d, $J = 1.77$ Hz, 1H), 7.57 (dd, $J = 9.09, 5.05$ Hz, 1H), 7.40–7.50 (m, 3H), 7.33–7.40 (m, 2H), 7.01 (d, $J = 1.77$ Hz, 1H), 6.15 (q, $J = 6.57$ Hz, 1H), 5.95 (s, 2H); 4.24 (m, 1H), 3.59 (m, 1H), 2.99–3.12 (m, 2H), 2.40–2.47 (m, 1H), 2.16–2.31 (m, 1H), 1.73–1.97 (m, 5H), 1.62–1.73 (m, 4H); 1.27–1.45 (m, 2H). HPLC purity (method A): $t_R = 6.293$, 100%.

4-(6-Amino-5-(1-(2,6-dichloro-3-fluorophenyl)ethoxy)pyridin-3-yl)-N-(2-(pyrrolidin-1-yl)ethyl)benzamide (37).

Acetic acid salt: LCMS m/z 517 (100%), 519 (64%) ($M + H$)⁺; ¹H NMR (400 MHz, DMSO- d_6) δ ppm 8.35–8.46 (m, 1H), 7.91 (d, $J = 2.02$ Hz, 1H), 7.78–7.88 (m, 2H), 7.57 (dd, $J = 8.84, 5.05$ Hz, 1H), 7.38–7.50 (m, 3H), 6.99 (d, $J = 1.52$ Hz, 1H), 6.07–6.20 (m, 1H), 6.00 (s, 2H), 3.35–3.41 (m, 4H), 2.57 (t, $J = 6.95$ Hz, 2H), 2.43–2.48 (m, 2H), 1.90 (s, 3H), 1.82 (d, $J = 6.57$ Hz, 3H), 1.68 (t, $J = 3.28$ Hz, 4H). HPLC purity (method A): $t_R = 7.801$, 99.4%.

(4-(6-Amino-5-(1-(2,6-dichloro-3-fluorophenyl)ethoxy)pyridin-3-yl)phenyl)((3S,5R)-3,5-dimethylpiperazin-1-yl)methanone (38). LCMS m/z 516, (100%), 518 (64%) ($M + H$)⁺; ¹H NMR (300 MHz, DMSO- d_6) δ ppm 7.88 (d, $J = 1.77$ Hz, 1H), 7.57 (dd, $J = 8.97, 4.93$ Hz, 1H), 7.40–7.49 (m, 3H), 7.31–7.40 (m, 2H), 7.00 (d, $J = 1.77$ Hz, 1H), 6.09–6.21 (m, 1H), 5.97 (s, 2H), 4.28–4.46 (m, 1H), 3.39–3.54 (m, 1H), 2.57–2.73 (m, 3H), 2.18–2.29 (m, 1H), 1.81 (d, $J = 6.57$ Hz, 3H), 0.78–1.05 (m, 6H). HPLC purity (method A): $t_R = 7.661$, 100%.

3-(1-(2,6-Dichloro-3-fluorophenyl)ethoxy)-5-(1-isopropyl-1H-pyrazol-4-yl)pyridin-2-amine (44). *Step 1.* To a solution of 4-(4,4,5,5-tetramethyl-1,3,2-dioxaborolan-2-yl)-1H-pyrazole (39, 1.00 g, 5.15 mmol) in DMF (25 mL, 0.2M) were added 2-iodopropane (0.55 mL, 5.15 mmol) and Cs₂CO₃ (2.50 g, 7.73 mmol). The mixture was stirred at 90 °C for 16 h, cooled, diluted with water, and extracted with EtOAc (3 × 50 mL). The combined organic layers were washed with brine, dried over Na₂SO₄, filtered, and concentrated to give 1-isopropyl-4-(4,4,5,5-tetramethyl-1,3,2-dioxaborolan-2-yl)-1H-pyrazole as a white solid (1.20 g, 100% yield); ¹H NMR (400 MHz, CDCl₃) δ ppm 7.80 (s, 1H), 7.75 (s, 1H), 4.53 (dt, $J = 13.39, 6.69$ Hz, 1H), 1.51 (d, $J = 6.57$ Hz, 6H), 1.32 (s, 12H).

Step 2. In a microwave vessel were added 1-isopropyl-4-(4,4,5,5-tetramethyl-1,3,2-dioxaborolan-2-yl)-1H-pyrazole (122 mg, 0.515 mmol), 3-(1-(2,6-dichloro-3-fluorophenyl)ethoxy)-5-iodopyridin-2-amine (200 mg, 0.468 mmol), DME (4 mL), and a freshly made solution of CsF (234 mg, 1.545 mmol) in water (1 mL). The reaction mixture was purged with N₂ for 5 min. Pd(PPh₃)₂Cl₂ (16.4 mg, 0.023 mmol) was added, and the system was purged with N₂ for 5 min. The mixture was heated in a microwave for 40 min at 120 °C. To the mixture were added EtOAc and water (10 mL each). The aqueous layer was extracted with EtOAc (3 × 10 mL), dried over Na₂SO₄, filtered, and concentrated. The crude material was purified with a reversed phase C-18 preparative HPLC column, eluting with acetonitrile/water with 0.1% acetic acid to afford 44 as a white amorphous solid (121 mg, 63% yield); LCMS m/z 409 (100%), 411 (64%) ($M + H$)⁺; ¹H NMR (400 MHz, CDCl₃) δ ppm 7.53–7.56 (m, 1H), 7.48 (s, 1H), 7.44 (d, $J = 1.77$ Hz, 1H), 7.37 (dd, $J = 8.84, 4.80$ Hz, 1H), 7.10–7.17 (m, 1H), 7.00–7.06 (m, 1H), 6.17 (q, $J = 6.82$ Hz, 1H), 4.42–4.60 (m, 1H), 1.91–1.97 (m, 3H), 1.51–1.57 (m, 6H). HPLC purity (method A): $t_R = 9.577$, 100%.

2-(4-(6-Amino-5-(1-(2,6-dichloro-3-fluorophenyl)ethoxy)pyridin-3-yl)-1H-pyrazol-1-yl)-N-(2-(dimethylamino)ethyl)-2-methylpropanamide (45). *Step 1.* To a solution of 4-(4,4,5,5-tetramethyl-1,3,2-dioxaborolan-2-yl)-1H-pyrazole (5 g, 25.77 mmol) and methyl 2-bromo-2-methylpropanoate (12.6 g, 27.06 mmol) in DMF (85 mL) was added Cs₂CO₃ (12.6 g, 38.65 mmol). The reaction mixture was heated in a 90 °C oil bath overnight. The reaction solution was cooled to room temperature and partitioned between water and ethyl acetate. The combined ethyl acetate solution was washed with water five times, dried over Na₂SO₄, and concentrated to give methyl 2-methyl-2-(4-(4,4,5,5-tetramethyl-1,3,2-dioxaborolan-2-yl)-1H-pyrazol-1-yl)propanoate (4.776 g, 63% yield); ¹H NMR (400 MHz, CDCl₃) δ ppm 7.89 (s, 1H), 7.84 (s, 1H), 3.71 (s, 3H), 1.85 (s, 6H), 1.32 (s, 12H).

Step 2. To a solution of 23 (6.363 g, 14.90 mmol) and methyl 2-methyl-2-(4-(4,4,5,5-tetramethyl-1,3,2-dioxaborolan-2-yl)-1H-pyrazol-1-yl)propanoate (4.6 g, 15.64 mmol) in DME (27 mL) was added a solution of CsF (6.79 g, 44.7 mmol) in water (9.3 mL). The reaction mixture was degassed 3 times with N₂. 1,1'-Bis(diphenylphosphino)ferrocene palladium

dichloride (545 mg, 0.745 mmol) was added, and the reaction mixture was degassed 3 times with N₂ and then microwaved at 120 °C for 1 h. The reaction solution was diluted with water and extracted with EtOAc. The combined extracts were dried over Na₂SO₄, concentrated, purified by a silica gel column chromatography with a gradient of 25–50% EtOAc/hexanes to provide methyl 2-(4-(6-amino-5-(1-(2,6-dichloro-3-fluorophenyl)ethoxy)pyridin-3-yl)-1H-pyrazol-1-yl)-2-methylpropanoate (1.46 g, 21% yield): LCMS *m/z* 467 (100%), 469 (64%) (M + H)⁺; ¹H NMR (400 MHz, CDCl₃) δ ppm 7.79 (d, *J* = 1.77 Hz, 1H), 7.62–7.66 (m, 2H), 7.30 (dd, *J* = 8.84, 4.80 Hz, 1H), 7.06 (t, *J* = 8.46 Hz, 1H), 6.89 (d, *J* = 1.52 Hz, 1H), 6.05–6.11 (m, 1H), 4.76–4.87 (m, 2H), 3.72–3.74 (m, 3H), 1.85–1.89 (m, 9H).

Step 3. To a solution of methyl 2-(4-(6-amino-5-(1-(2,6-dichloro-3-fluorophenyl)ethoxy)pyridin-3-yl)-1H-pyrazol-1-yl)-2-methylpropanoate (2.92 g, 6.25 mmol) in MeOH (31 mL) was added a solution of LiOH (450 mg, 18.76 mmol) in water (6.25 mL). The mixture was heated at 60 °C for 45 min and cooled to ambient temperature. The pH of the reaction solution was adjusted to ~5 with 1 N HCl, and the product was precipitated out. 2-(4-(6-Amino-5-(1-(2,6-dichloro-3-fluorophenyl)ethoxy)pyridin-3-yl)-1H-pyrazol-1-yl)-2-methylpropanoic acid was obtained after filtration (2.825 g, 100% yield): ¹H NMR (400 MHz, DMSO-*d*₆) δ ppm 8.09 (s, 1H), 7.82 (d, *J* = 1.52 Hz, 1H), 7.57–7.62 (m, 2H), 7.43–7.48 (m, 1H), 6.98 (s, 1H), 5.94–6.24 (m, 3H), 1.83 (d, *J* = 6.57 Hz, 3H), 1.75 (s, 6H).

Step 4. To a solution of 2-(4-(6-amino-5-(1-(2,6-dichloro-3-fluorophenyl)ethoxy)pyridin-3-yl)-1H-pyrazol-1-yl)-2-methylpropanoic acid (1.00 g, 2.20 mmol) in DMF (5.5 mL) were added HOBT (300 mg, 2.20 mmol), EDC (633 mg, 3.30 mmol), and N¹,N¹-dimethylethane-1,2-diamine (225 mg, 2.20 mmol). The mixture was stirred overnight and then purified by a reversed phase C-18 preparative HPLC column, eluting with acetonitrile/water with 0.1% acetic acid to afford **45** as a white solid (170 mg, 14% yield): LCMS *m/z* 523 (100%), 525 (64%) (M + H)⁺. ¹H NMR (400 MHz, CDCl₃) δ ppm 7.65–7.72 (m, 2H), 7.64 (s, 1H), 7.32 (dd, *J* = 8.84, 4.80 Hz, 1H), 7.07 (t, *J* = 8.34 Hz, 1H), 6.90–6.96 (m, 1H), 6.87 (d, *J* = 1.52 Hz, 1H), 6.04–6.11 (m, 1H), 5.25 (br s, 2H), 3.43–3.51 (m, 2H), 2.80 (t, *J* = 5.68 Hz, 2H), 2.51 (s, 6H), 2.06 (s, 3H), 1.81–1.92 (m, 9H). HPLC purity (method B): *t*_R = 3.156, 95.2%.

2-(4-(6-Amino-5-(1-(2,6-dichloro-3-fluorophenyl)ethoxy)pyridin-3-yl)-1H-pyrazol-1-yl)-N-(3-(dimethylamino)propyl)acetamide (46). Compound **46** was prepared with similar procedures as compound **45**: LCMS (APCI) *m/z* 509 (100%), 511 (64%) (M + H)⁺. ¹H NMR (400 MHz, CDCl₃) δ ppm 7.78 (d, *J* = 1.77 Hz, 1H), 7.70–7.77 (m, 1H), 7.67 (s, 1H), 7.50 (s, 1 H), 7.31 (dd, *J* = 8.84, 4.80 Hz, 1H), 7.01–7.09 (m, 1H), 6.86 (d, *J* = 1.77 Hz, 1H), 6.07 (q, *J* = 6.65 Hz, 1H), 4.74–4.86 (m, 4H), 3.30–3.41 (m, 2H), 2.22–2.34 (m, 2H), 1.94 (s, 6H), 1.87 (d, *J* = 6.57 Hz, 3H), 1.57 (dt, *J* = 11.94, 6.03 Hz, 2H). Anal. Calcd for C₂₃H₂₇N₆O₂Cl₂F · 1.5H₂O: C, 51.50; H, 5.64; N, 15.67. Found: C, 51.47; H, 5.39; N, 15.70.

4-((4-(6-Amino-5-(1-(2,6-dichloro-3-fluorophenyl)ethoxy)pyridin-3-yl)-1H-pyrazol-1-yl)methyl)-tetrahydro-2H-pyran-4-ol (47). **Step 1:** *tert*-Butyl 1-Oxa-6-azaspiro[2.5]octane-6-carboxylate (**52**). To a solution of dimethylsulfoxonium methylide, which was prepared under N₂ from NaH of 60% dispersion in mineral oil (440 mg, 11.0 mmol) and trimethylsulfoxonium iodide (2.421 g, 11.0 mmol) in 5 mL of anhydrous DMSO, was added 1-Boc-4-oxo-1-piperidincarboxylate (**50**, 1.993 g, 10.0 mmol) in 5 mL of DMSO dropwise. The resulting mixture was stirred at 55 °C for 6 h. The cooled reaction mixture was poured into ice–water and extracted with EtOAc (2 × 200 mL). The combined organic layers were washed with H₂O (50 mL), brine (50 mL) and then dried over Na₂SO₄. After concentration, **52** was obtained as a yellow oil (1.479 g, 69% yield): ¹H NMR (400 MHz, CDCl₃) δ ppm 3.62–3.78 (m, 2H), 3.35–3.49 (m, 2 H), 2.63–2.72 (m, 2 H), 1.71–1.84 (m, 2 H), 1.37–1.52 (m, 11 H).

Step 2: *tert*-Butyl 4-Hydroxy-4-((4-(4,4,5,5-tetramethyl-1,3,2-dioxaborolan-2-yl)-1H-pyrazol-1-yl)methyl)piperidine-1-carboxylate (**53**). A reaction mixture of **52** (214 mg, 1.0 mmol) and 4-(4,4,5,5-tetramethyl-1,3,2-dioxaborolan-2-yl)-1H-pyrazole (**39**, 194 mg, 1.0 mmol) with NaH of 60% dispersion in mineral oil (60 mg, 1.5 mmol) in DMF (3 mL) was stirred at 90 °C for 3 h. The reaction mixture was partitioned between EtOAc (200 mL) and saturated NaHCO₃ solution (50 mL) and washed with brine (50 mL). The organic layer was dried over Na₂SO₄ and concentrated to give **53** as a yellow grease (361 mg, 89% yield): LCMS *m/z* 408 (M + H)⁺; ¹H NMR (400 MHz, CDCl₃) δ ppm 8.00 (s, 1H), 7.80 (s, 1H), 7.65 (s, 1H), 4.05 (s, 2H), 3.72–3.91 (m, 2H), 3.13–3.15 (m, 2H), 1.56–1.78 (m, 4H), 1.45 (s, 9H), 1.30 (s, 12H).

Step 3: 4-((4-(6-Amino-5-(1-(2,6-dichloro-3-fluorophenyl)ethoxy)pyridin-3-yl)-1H-pyrazol-1-yl)methyl)tetrahydro-2H-pyran-4-ol (**47**). To a reaction mixture of **53** (361 mg, 0.89 mmol) and **23** (378 mg, 0.89 mmol) in ethylene glycol dimethyl ether (DME) (9 mL) were added Na₂CO₃ solution (1.0 N, 3.9 mL, 3.9 mmol) and Pd(II)-(PPh₃)₂Cl₂ (32 mg, 0.05 mmol). The reaction mixture was purged with N₂ for 15 min and stirred at 85 °C under N₂ overnight. The mixture was partitioned between EtOAc (200 mL) and saturated NaHCO₃ solution (2 × 50 mL) and washed with brine (50 mL). The organic layer was dried over Na₂SO₄, concentrated, and purified by a reversed phase C-18 preparative HPLC column, eluting with 25–95% MeCN in H₂O with 0.1% HOAc. *tert*-Butyl 4-((4-(6-amino-5-(1-(2,6-dichloro-3-fluorophenyl)ethoxy)pyridin-3-yl)-1H-pyrazol-1-yl)methyl)-4-hydroxypiperidine-1-carboxylate was obtained as a white solid (147 mg, 28% yield), which was dissolved in 5 mL of CH₂Cl₂. To the solution was added 4.0 M HCl in dioxane (2.0 mL, 8.1 mmol). The reaction mixture was stirred at ambient temperature for 2.0 h, concentrated, and purified with reversed phase C-18 preparative HPLC column, eluting with 5–95% MeCN in H₂O with 0.1% HOAc, and **47** was obtained as an off-white solid (76 mg, 63% yield): LCMS *m/z* 481 (100%), 483 (64%) (M + H)⁺; ¹H NMR (400 MHz, CDCl₃) δ ppm 7.65–7.69 (m, 1H), 7.57–7.62 (m, 1H), 7.44–7.49 (m, 1H), 7.32 (dd, *J* = 8.84, 4.80 Hz, 1H), 7.08 (d, *J* = 8.08 Hz, 1H), 6.87 (d, *J* = 1.77 Hz, 1H), 6.04–6.14 (m, 1H), 5.44 (br s, 2H), 4.09 (s, 2H), 3.72–3.85 (m, 4H), 1.87 (d, *J* = 6.57 Hz, 3H), 1.59–1.69 (m, 2H), 1.32–1.40 (m, 2H). HPLC purity (method B): *t*_R = 0.765, 95.1%.

5-(1-(Azetidin-3-yl)-1H-pyrazol-4-yl)-3-(1-(2,6-dichloro-3-fluorophenyl)ethoxy)pyridin-2-amine (50). **Step 1:** *tert*-Butyl 3-(Methylsulfonyloxy)azetidine-1-carboxylate. To a solution of *tert*-butyl 3-hydroxyazetidine-1-carboxylate (466 mg, 2.69 mmol), Et₃N (0.75 mL, 5.38 mmol), and 4-(dimethylamino)pyridine (33 mg, 0.269 mmol) in CH₂Cl₂ (10 mL) at 0 °C was added methanesulfonyl chloride (0.25 mL, 3.23 mmol). The resulting brown mixture was stirred at 0 °C to ambient temperature overnight. The reaction was quenched with NaHCO₃, and then the mixture was partitioned between CH₂Cl₂ (200 mL) and saturated NaHCO₃ solution (50 mL). The organic layer was dried over Na₂SO₄, filtered through a silica gel pad, and eluted with hexane/EtOAc, 1:1. The filtrate was concentrated by vacuum to give *tert*-butyl 3-(methylsulfonyloxy)azetidine-1-carboxylate as a yellow oil (614 mg, 91% yield): ¹H NMR (400 MHz, CDCl₃) δ ppm 5.26–5.11 (m, 1H), 4.26 (dd, *J* = 10.36, 6.82 Hz, 2H), 4.08 (dd, *J* = 10.36, 4.29 Hz, 2H), 3.05 (s, 3H), 1.43 (s, 9H).

Step 2: *tert*-Butyl 3-(4-Bromo-1H-pyrazol-1-yl)azetidine-1-carboxylate. A microwave tube (5 mL) was charged with *tert*-butyl 3-(methylsulfonyloxy)azetidine-1-carboxylate (304 mg, 1.21 mmol), 4-bromopyrazole (178 mg, 1.21 mmol), NaH 60% in mineral oil (73 mg, 1.82 mmol), and anhydrous DMF (2 mL). The resulting mixture was microwaved at 110 °C for 30 min and then partitioned between EtOAc (200 mL) and saturated NaHCO₃ solution (2 × 50 mL) and washed with brine (50 mL). The organic layer was dried over Na₂SO₄ and concentrated by vacuum to afford *tert*-butyl 3-(4-bromo-1H-pyrazol-1-yl)azetidine-1-carboxylate as a yellow oil (360 mg, 98%): ¹H NMR (400 MHz, DMSO-*d*₆)

δ ppm 8.14 (s, 1H), 7.67 (s, 1H), 5.22–5.12 (m, 1H), 4.31–4.18 (m, 2H), 4.08 (s, 2H), 1.43–1.36 (m, 9H).

Step 3: *tert*-Butyl 3-(4-(4,4,5,5-tetramethyl-1,3,2-dioxaborolan-2-yl)-1H-pyrazol-1-yl)azetidine-1-carboxylate. A reaction mixture of *tert*-butyl 3-(4-bromo-1H-pyrazol-1-yl)azetidine-1-carboxylate (225 mg, 0.74 mmol) and bis(pinacolato)diboron (227 mg, 0.89 mmol) with KOAc (247 mg, 2.52 mmol) in DMSO (3 mL) was purged with N₂ for 15 min. Then PdCl₂(dppf)₂CH₂Cl₂ (30 mg, 2.52 mmol) was added. The resulting mixture was stirred at 80 °C under N₂ overnight. After it cooled to room temperature, the mixture was filtered through a Celite pad and washed well with EtOAc. The filtrate was washed with H₂O (2 × 50 mL) and brine (50 mL). The organic layer was dried over Na₂SO₄ and then concentrated by vacuum. The residue was purified on a silica gel column, eluting with hexane/EtOAc (3:2) to provide *tert*-butyl 3-(4-(4,4,5,5-tetramethyl-1,3,2-dioxaborolan-2-yl)-1H-pyrazol-1-yl)azetidine-1-carboxylate as a clear oil (250 mg, 97% yield): ¹H NMR (400 MHz, CDCl₃) δ ppm 7.83 (s, 2H), 5.13–4.98 (m, 1H), 4.36 (t, *J* = 8.59 Hz, 2H), 4.33–4.22 (m, 2H), 1.49–1.41 (m, 6H), 1.34–1.28 (m, 6H), 1.27–1.18 (m, 9H).

Step 4: *tert*-Butyl 3-(4-(6-amino-5-(1-(2,6-dichloro-3-fluorophenyl)ethoxy)pyridin-3-yl)-1H-pyrazol-1-yl)azetidine-1-carboxylate. A reaction mixture of *tert*-butyl 3-(4-(4,4,5,5-tetramethyl-1,3,2-dioxaborolan-2-yl)-1H-pyrazol-1-yl)azetidine-1-carboxylate (459 mg, 1.31 mmol) and 3-[1-(2,6-dichloro-3-fluorophenyl)ethoxy]-5-iodopyridin-2-amine (27, 374 mg, 0.88 mmol) in 13 mL of ethylene glycol dimethyl ether (13 mL) was purged with N₂ for 15 min. Then Pd(II)(PPh₃)₂Cl₂ (46 mg, 0.07 mmol) was added and purging continued with N₂ for another 15 min. Another 1.0 N Na₂CO₃ solution (3.9 mL, 3.9 mmol) was added after purging with N₂ for 15 min. The resulting mixture was stirred at 85 °C under N₂ overnight. The reaction mixture was filtered through a Celite pad and washed well with MeOH. The filtrate was concentrated by vacuum. The residue was partitioned between EtOAc (200 mL) and saturated NaHCO₃ solution (2 × 50 mL) and washed with brine (50 mL). The organic layer was dried over Na₂SO₄, concentrated, and purified by a flash chromatography, eluting with 0–10% methanol in CH₂Cl₂ to afford *tert*-butyl 3-(4-(6-amino-5-(1-(2,6-dichloro-3-fluorophenyl)ethoxy)pyridin-3-yl)-1H-pyrazol-1-yl)azetidine-1-carboxylate as a brown grease (421 mg, 92% yield): LCMS *m/z* 522 (100%), 524 (64%) (M + H)⁺; ¹H NMR (400 MHz, CDCl₃) δ ppm 7.78–7.72 (m, 1H), 7.65–7.59 (m, 1H), 7.58–7.53 (m, 1H), 7.52–7.44 (m, 1H), 7.41–7.33 (m, 1H), 7.04 (t, *J* = 8.46 Hz, 1H), 5.02 (d, *J* = 7.58 Hz, 1H), 4.79 (s, 2H), 4.41–4.34 (m, 1H), 4.33–4.20 (m, 2H), 4.18–4.04 (m, 2H), 1.87–1.80 (m, 3H), 1.26–1.17 (m, 9H).

Step 5: 5-(1-Azetidin-3-yl-1H-pyrazol-4-yl)-3-[1-(2,6-dichloro-3-fluorophenyl)ethoxy]pyridin-2-amine (50). A reaction mixture of *tert*-butyl 3-(4-(6-amino-5-(1-(2,6-dichloro-3-fluorophenyl)ethoxy)pyridin-3-yl)-1H-pyrazol-1-yl)azetidine-1-carboxylate (421 mg, 0.81 mmol) with dry HCl in dioxane (4.0 M, 2.0 mL, 8.1 mmol) in CH₂Cl₂ (5 mL) was stirred at ambient temperature for 2.0 h. The reaction mixture was concentrated by vacuum. The residue was treated with EtOAc. The precipitated solid was filtered off and washed well with EtOAc, hexane, then dried under vacuum to give 50 as a sand color solid of HCl salt (275 mg, 81% yield), which was further purified on a reversed phase HPLC column, eluting with acetonitrile in water with 0.1% acetic acid to provide 50 as a white amorphous solid after lyophilization: LCMS *m/z* 422 (100%), 424 (64%) (M + H)⁺; ¹H NMR (400 MHz, DMSO-*d*₆) δ ppm 9.20 (s, 1H), 8.12 (s, 1H), 7.86 (s, 1H), 7.73–7.83 (m, 1H), 7.59 (dd, *J* = 8.84, 5.05 Hz, 1H), 7.40–7.54 (m, 1H), 7.09 (s, 1H), 6.23 (d, *J* = 6.57 Hz, 2H), 5.40 (s, 1H), 4.35 (s, 4H), 3.56 (s, 1H), 1.79–1.89 (m, 3H). Anal. Calcd for C₁₉H₁₈N₅OCl₂F · 2H₂O · 1CH₃CO₂H: C, 48.66; H, 5.06; N, 13.51. Found: C, 48.41; H, 4.89; N, 13.14.

Compounds 48 and 49 were prepared with similar procedures as compound 50.

5-(1-(Azetidin-3-ylmethyl)-1H-pyrazol-4-yl)-3-(1-(2,6-dichloro-3-fluorophenyl)ethoxy)pyridin-2-amine (48). Yield:

78%. LCMS *m/z* 436 (100%), 438 (64%) (M + H)⁺; ¹H NMR (400 MHz, MeOD) δ ppm 7.69 (s, 1H), 7.57 (s, 1H), 7.48 (s, 1H), 7.35 (dd, *J* = 8.84, 4.80 Hz, 1H), 7.14 (t, *J* = 8.59 Hz, 1H), 6.83 (s, 1H), 6.08 (d, *J* = 6.57 Hz, 1H), 4.29 (d, *J* = 6.82 Hz, 2H), 4.00 (t, *J* = 9.73 Hz, 2H), 3.84–3.95 (m, 2H), 3.32 (d, *J* = 8.08 Hz, 1H), 1.78 (d, *J* = 6.57 Hz, 3H). Anal. Calcd for C₂₀H₂₀N₅OCl₂F · 2.5HCl · 2H₂O · 2.5CH₃CO₂H: C, 42.08; H, 5.16; N, 9.81. Found: C, 42.34; H, 4.98; N, 9.41.

1-(3-((4-(6-amino-5-(1-(2,6-dichloro-3-fluorophenyl)ethoxy)pyridin-3-yl)-1H-pyrazol-1-yl)methyl)azetidin-1-yl)-2-(dimethylamino)ethanone (49). LCMS *m/z* 521 (100%), 523 (64%) (M + H)⁺; ¹H NMR (400 MHz, DMSO-*d*₆) δ ppm 7.91 (d, *J* = 1.52 Hz, 1H), 7.74 (d, *J* = 1.77 Hz, 1H), 7.52–7.61 (m, 2H), 7.40–7.47 (m, 1H), 6.88 (s, 1H), 6.08 (q, *J* = 6.57 Hz, 1H), 5.66 (s, 2H), 4.31 (d, *J* = 7.33 Hz, 2H), 4.21 (t, *J* = 8.59 Hz, 1H), 3.98 (dd, *J* = 8.97, 5.43 Hz, 1H), 3.90 (t, *J* = 9.09 Hz, 1H), 3.68 (dd, *J* = 9.98, 5.43 Hz, 1H), 2.84–2.92 (m, 2H), 2.15 (s, 6H), 1.80 (d, *J* = 6.57 Hz, 3H). HPLC purity (method A): *t*_R = 6.731, 100%.

3-(1-(2,6-Dichloro-3-fluorophenyl)ethoxy)-5-(1-(piperidin-4-yl)-1H-pyrazol-4-yl)pyridin-2-amine (61). **Step 1.** To a solution of 5-bromo-3-[1-(2,6-dichloro-3-fluorophenyl)ethoxy]pyridin-2-ylamine (22, 12.83 g, 33.76 mmol) in anhydrous DMF (100 mL) were added di-*tert*-butyl dicarbonate (21.25 g, 97.35 mmol) and 4-dimethylaminopyridine (0.793 g, 6.49 mmol). The mixture was stirred at ambient temperature for 18 h. Saturated NaHCO₃ solution (300 mL) was added to the mixture and extracted with EtOAc (3 × 250 mL). The combined extracts were washed with water (5 × 100 mL), saturated NaHCO₃, and brine, then dried over Na₂SO₄. After filtration, evaporation, and high vacuum drying, 54 was obtained as an off-white foam solid (19.59 g, 100% yield): ¹H NMR (400 MHz, DMSO-*d*₆) δ ppm 8.18 (d, *J* = 1.77 Hz, 1H), 7.83 (d, *J* = 2.02 Hz, 1H), 7.52–7.61 (m, 1H), 7.43–7.52 (m, 1H), 6.21–6.33 (m, 1H), 1.75 (d, *J* = 6.57 Hz, 3H), 1.39 (s, 9H), 1.16–1.27 (m, 9H).

Step 2. To a solution of 54 (19.58 g, 33.76 mmol) in DMSO (68 mL) was added potassium acetate (11.26 g, 114.78 mmol) and bis-(pinacolato)diboron (10.29 g, 40.51 mmol). The mixture was degassed and charged with nitrogen three times. Then Pd(dppf)Cl₂ · CH₂Cl₂ (1.38 g, 1.69 mmol) was added. The reaction mixture was degassed and charged with nitrogen three times and then stirred in a 80 °C oil bath for 12 h. The reaction was cooled to ambient temperature, diluted with ethyl acetate (100 mL), and filtered through a Celite pad which was washed with ethyl acetate. The combined ethyl acetate solution (700 mL) was washed with water (5 × 100 mL), brine (100 mL) and dried over Na₂SO₄. After filtration and concentration, the residue was purified on a silica gel column, eluting with EtOAc/hexane (0–50%) to provide 56 as a foam solid (20.59 g, 97% yield): ¹H NMR (400 MHz, DMSO-*d*₆) δ ppm 8.18 (d, *J* = 1.26 Hz, 1H), 7.51–7.61 (m, 2H), 7.42–7.50 (m, 1H), 6.12–6.21 (m, 1H), 1.74 (d, *J* = 6.57 Hz, 3H), 1.16–1.42 (m, 30H).

Step 3. To a solution of 56 (20.34 g, 32.42 mmol) in CH₂Cl₂ (80 mL) was added a solution of dry HCl in dioxane (4 N, 40.5 mL, 162 mmol). The reaction solution was stirred in a 40 °C oil bath for 12 h. The reaction mixture was cooled to ambient temperature, diluted with EtOAc (400 mL), then washed carefully but quickly with saturated NaHCO₃ until the water layer was basic (pH > 8). The organic layer was washed with brine and dried over Na₂SO₄. After filtration, evaporation, and high vacuum drying, 57 was obtained as an off-white foam solid (13.48 g, 97% yield): ¹H NMR (400 MHz, DMSO-*d*₆) δ ppm 7.71–7.78 (m, 1H), 7.54 (dd, *J* = 8.97, 4.93 Hz, 1H), 7.36–7.49 (m, 1H), 6.87 (d, *J* = 1.01 Hz, 1H), 6.13 (br s, 2H), 5.99 (q, *J* = 6.65 Hz, 1H), 1.77 (d, *J* = 6.82 Hz, 3H), 1.22 (s, 6 H) 1.20 (s, 6 H).

Step 4. To a stirred solution of 57 (4.2711 g, 10.0 mmol) and *tert*-butyl 4-(4-bromo-1H-pyrazol-1-yl)piperidine-1-carboxylate (3.9628 g, 12.0 mmol) in DME (40 mL) was added a solution of Na₂CO₃ (3.1787 g, 30.0 mmol) in water (10 mL). The solution was degassed and charged with nitrogen three times. To the solution was added Pd(PPh₃)₂Cl₂

(351 mg, 0.50 mmol). The reaction solution was degassed and charged with nitrogen again three times and then stirred in an 87 °C oil bath for 16 h. After cooling to ambient temperature, the reaction mixture was diluted with EtOAc (200 mL), filtered through a pad of Celite, and washed with EtOAc. The combined EtOAc solution was washed with brine, dried over Na₂SO₄, and concentrated. The crude product was purified on a silica gel column, eluting with EtOAc/hexane system (0–100% EtOAc) to afford *tert*-butyl 4-(4-(6-amino-5-(1-(2,6-dichloro-3-fluorophenyl)ethoxy)pyridin-3-yl)-1H-pyrazol-1-yl)piperidine-1-carboxylate as a foam solid (3.4167 g, 65% yield).

Step 5. To a solution of *tert*-butyl 4-(4-(6-amino-5-(1-(2,6-dichloro-3-fluorophenyl)ethoxy)pyridin-3-yl)-1H-pyrazol-1-yl)piperidine-1-carboxylate (566.7 mg, 1.03 mmol) in methanol (5 mL) was added 4 N HCl in dioxane (1 mL, 4 mmol). The solution was stirred for about 1 h or until the deprotection was complete. The solvents were evaporated and the residue was dissolved in methanol and purified on a reversed phase C-18 preparative HPLC column, eluting with acetonitrile/water with 0.1% acetic acid from 5% to 30% with a linear gradient. After lyophilization, **61** was obtained as a white solid (410 mg, 78% yield): LCMS *m/z* 450 (100%), 452 (64%) (*M* + *H*)⁺; ¹H NMR (400 MHz, DMSO-*d*₆) δ ppm 7.92 (s, 1H), 7.75 (d, *J* = 1.77 Hz, 1H), 7.58 (dd, *J* = 8.97, 4.93 Hz, 1H), 7.52 (s, 1H), 7.42–7.48 (m, 1H), 6.89 (d, *J* = 1.77 Hz, 1H), 6.03–6.14 (m, 1H), 5.65 (s, 2H), 4.08–4.20 (m, 1H), 2.99–3.07 (m, 2H), 2.57 (td, *J* = 12.38, 2.27 Hz, 2H), 1.90–1.97 (m, 2H), 1.80 (d, *J* = 6.82 Hz, 3H), 1.74 (dd, *J* = 12.00, 3.92 Hz, 2H). HPLC purity (method A): *t*_R = 6.694, 100%.

Compounds **58–60** were prepared by using similar procedures described for the synthesis of compound **61**.

3-(1-(2,6-Dichloro-3-fluorophenyl)ethoxy)-5-(1-((S)-pyrrolidin-3-yl)-1H-pyrazol-4-yl)pyridin-2-amine (58). LCMS *m/z* 436 (100%), 438 (64%) (*M* + *H*)⁺; ¹H NMR (400 MHz, CDCl₃) δ ppm 7.65 (s, 1H), 7.56 (s, 1H), 7.46 (s, 1H), 7.39 (dd, *J* = 8.59, 5.05 Hz, 1H), 7.15 (t, *J* = 8.08 Hz, 1H), 6.99–7.03 (m, 1H), 6.13–6.22 (m, 1H), 5.06–5.13 (m, 1H), 3.74–3.84 (m, 2H), 3.57–3.72 (m, 2H), 2.55–2.70 (m, 1H), 2.33–2.47 (m, 1H), 1.95 (d, *J* = 6.82 Hz, 3H). HPLC purity (method B): *t*_R = 2.872, 100%.

3-(1-(2,6-Dichloro-3-fluorophenyl)ethoxy)-5-(1-(piperidin-3-yl)-1H-pyrazol-4-yl)pyridin-2-amine (59). LCMS *m/z* 450 (100%), 452 (64%) (*M* + *H*)⁺; ¹H NMR (400 MHz, CDCl₃) δ ppm 7.70 (d, *J* = 1.52 Hz, 1H), 7.56 (s, 1H), 7.53 (s, 1H), 7.32 (dd, *J* = 8.84, 4.80 Hz, 1H), 7.02–7.10 (m, 1H), 6.87 (d, *J* = 1.77 Hz, 1H), 6.03–6.13 (m, 1H), 5.22 (br s, 2H), 4.18–4.31 (m, 1H), 3.37–3.44 (m, 1H), 3.03–3.12 (m, 2H), 2.72–2.83 (m, 1H), 1.98–2.05 (m, 3H), 1.87 (d, *J* = 6.57 Hz, 3H), 1.60–1.72 (m, 1H). HPLC purity (method B): *t*_R = 2.892, 100%.

3-(1-(2,6-Dichloro-3-fluorophenyl)ethoxy)-5-(1-(tetrahydro-2H-pyran-4-yl)-1H-pyrazol-4-yl)pyridin-2-amine (60). LCMS *m/z* 451 (100%), 453 (64%) (*M* + *H*)⁺; ¹H NMR (400 MHz, DMSO-*d*₆) δ ppm 7.96 (s, 1H), 7.76 (d, *J* = 1.77 Hz, 1H), 7.54–7.63 (m, 2H), 7.41–7.48 (m, 1H), 6.90 (d, *J* = 1.52 Hz, 1H), 6.06–6.13 (m, 1H), 5.65 (s, 2H), 4.30–4.41 (m, 1H), 3.90–4.01 (m, 2H), 3.43–3.53 (m, 2H), 1.93–2.00 (m, 2H), 1.84–1.91 (m, 2H), 1.81 (d, *J* = 6.82 Hz, 3H). HPLC purity (method A): *t*_R = 8.712, 100%.

3-((R)-1-(2,6-Dichloro-3-fluorophenyl)ethoxy)-5-(1-(piperidin-4-yl)-1H-pyrazol-4-yl)pyridin-2-amine (Crizotinib). To a stirred solution of *tert*-butyl 4-hydroxypiperidine-1-carboxylate (7.94 g, 39.45 mmol) in CH₂Cl₂ (100 mL), cooled to 0 °C, was slowly added Et₃N (5.54 mL, 39.45 mmol) followed by methane sulfonyl chloride (3.06 mL, 39.45 mmol) and DMAP (48 mg, 0.39 mmol). The mixture was stirred at room temperature overnight. To the mixture was added water (30 mL). Extraction with CH₂Cl₂ (3 × 30 mL) followed by drying (Na₂SO₄) and removal of the solvent in vacuo afforded *tert*-butyl 4-(methylsulfonyloxy)piperidine-1-carboxylate **65** as a white solid (11.00 g, >99% yield): ¹H NMR (400 MHz, CDCl₃) δ 4.89 (m, 1H), 3.69 (m, 2H), 3.31 (m, 2H), 3.04 (s, 3H), 1.95 (m, 2H), 1.83 (m, 2H), 1.46 (s, 9H).

NaH (16.32 g, 0.68 mol) was added portionwise to a stirred solution of 4-iodopyrazole (**66**, 110.57 g, 0.57 mol) in DMF (2 L) at 4 °C. The resulting mixture was stirred for 1 h at 4 °C, and **65** (176.00 g, 0.63 mol) was then added. The resulting mixture was heated to 100 °C for 12 h. The reaction was quenched with H₂O, and the aqueous portion was extracted with EtOAc several times. The combined organic layers were dried over Na₂SO₄, filtered, and concentrated to afford an orange oil. The residue was purified by a silica gel column, eluting with 5% EtOAc in pentane to give *tert*-butyl 4-(4-iodo-1H-pyrazol-1-yl)piperidine-1-carboxylate **67** as a white solid (140 g, 66%): ¹H NMR (400 MHz, DMSO-*d*₆) δ ppm 7.98 (s, 1H), 7.52 (s, 1H), 4.30–4.43 (m, 1H), 3.93–4.07 (m, 2H), 2.77–2.97 (m, 2H), 1.90–2.00 (m, 2H), 1.66–1.83 (m, 2H), 1.40 (s, 9H).

Bis(pinacolato)diboron (**55**, 134 g, 0.52 mol) and potassium acetate (145 g, 1.48 mol) were added sequentially to a solution of **67** (140 g, 0.37 mol) in DMSO (1.5 L). The mixture was purged with nitrogen several times, and dichlorobis(triphenylphosphino)palladium(II) (12.9 g, 0.018 mol) was then added. The resulting mixture was heated at 80 °C for 2 h. The reaction mixture was cooled to ambient temperature and filtered through a bed of Celite and washed with EtOAc. The filtrate was washed with brine (2 × 500 mL), dried over Na₂SO₄, filtered, and concentrated. The residue was purified by a silica gel column, eluting with 5% EtOAc in hexanes to give **68** as a white solid (55 g, 40%): ¹H NMR (400 MHz, DMSO-*d*₆) δ ppm 7.97 (s, 1H), 7.59 (s, 1H), 4.29–4.44 (m, 1H), 4.01 (d, *J* = 13.14 Hz, 2H), 2.77–3.01 (m, 2H), 1.92–1.99 (m, 2H), 1.78 (dd, *J* = 12.00, 4.17 Hz, 2H), 1.41 (s, 9H), 1.24 (s, 12H).

A reaction solution of (*R*)-5-bromo-3-(1-(2,6-dichloro-3-fluorophenyl)ethoxy)pyridin-2-amine (**69**, 14.4 g, 37.9 mmol) and **68** (17.2 g, 45.5 mmol) in DME (114 mL) was purged with nitrogen. Then Pd(dppf)Cl₂ (1.24 g, 1.52 mmol) and Cs₂CO₃ aqueous solution (2.0 N, 57 mL, 114 mmol) were added. The resulting mixture was purged with nitrogen and stirred at 90 °C for 3 h. The reaction mixture was cooled to ambient temperature and filtered through a Celite pad and washed well with MeOH. The filtrate was concentrated by vacuum. The residue was partitioned between EtOAc (800 mL) and saturated NaHCO₃ solution (2 × 150 mL) and brine (150 mL). The organic layer was dried over Na₂SO₄ and then filtered through a silica gel pad and washed well with EtOAc to remove black solid. The filtrate was concentrated by vacuum. The residue was purified by a silica gel column, eluting with EtOAc/hexane system to collect desired fraction and then concentrated by vacuum. The residue of off-white foam was treated with ether (100 mL) and hexane (500 mL). The precipitated solid was filtered off and washed well with hexane, then dried under vacuum to afford *tert*-butyl 4-(4-(6-amino-5-((*R*)-1-(2,6-dichloro-3-fluorophenyl)ethoxy)pyridin-3-yl)-1H-pyrazol-1-yl)piperidine-1-carboxylate as an off-white solid (19.55 g, 94% yield).

To a solution of 4-(4-(6-amino-5-((*R*)-1-(2,6-dichloro-3-fluorophenyl)ethoxy)pyridin-3-yl)-1H-pyrazol-1-yl)piperidine-1-carboxylate (19.54 g, 35.5 mmol) in CH₂Cl₂ (250 mL) at 0 °C was added 4.0 N HCl in dioxane (133 mL, 532 mmol) dropwise. The resulting mixture was stirred at 0 °C to room temperature for 4 h. The white suspension was filtered off, and the yellowish crude product was dissolved in H₂O (500 mL) and extracted with CH₂Cl₂ (500 mL). The pH of the aqueous layer was adjusted to ~10 by adding Na₂CO₃, and then the aqueous portion was extracted with EtOAc (1000 mL). The organic layer was washed with saturated aqueous NaHCO₃ (400 mL) and brine (150 mL), then dried over Na₂SO₄, and concentrated by vacuum. The precipitated solid was treated with ether and hexane and filtered off, washed well with ether and hexane, then dried under vacuum to afford crizotinib (**63**) as a white powder (15.34 g, 96% yield): mp 196–199 °C; LCMS *m/z* 450 (100%), 452 (64%) (*M* + *H*)⁺; ¹H NMR (400 MHz, DMSO-*d*₆) δ ppm 7.92 (s, 1H), 7.75 (d, *J* = 1.77 Hz, 1H), 7.58 (dd, *J* = 8.97, 4.93 Hz, 1H), 7.52 (s, 1H), 7.42–7.48 (m, 1H), 6.89 (d, *J* = 1.77 Hz, 1H), 6.03–6.14 (m, 1H), 5.65 (s, 2H), 4.08–4.20 (m, 1H), 2.99–3.07 (m, 2H), 2.57 (td, *J* = 12.38, 2.27 Hz, 2H), 1.90–1.97 (m, 2H), 1.80 (d, *J* = 6.82 Hz, 3H), 1.74 (dd, *J* = 12.00, 3.92

Hz, 2H). HPLC purity (method A): $t_R = 6.694$, 100%. Anal. Calcd for $C_{21}H_{22}N_5OCl_2F \cdot 0.5H_2O$: C, 54.91; H, 5.05; N, 15.25. Found: C, 55.20; H, 4.91; N, 15.13.

Biochemical Kinase Assays. c-MET enzyme inhibition was measured by Omnia (Invitrogen Inc.) continuous fluorometric assay as described previously.²⁴ The reactions were conducted in 50 μ L volumes in 96-well plates at 30 °C. Mixtures contained 1 nM human recombinant c-MET kinase domain (aa 1051–1348), 2 μ M phosphoacceptor peptide Ac-EEEEYI(cSx)-IV-NH₂ (Invitrogen Inc.), test compound (11-dose 3-fold serial dilutions, 2% DMSO final) or DMSO only, 0.2 mM DTT, and 10 mM MgCl₂ in 20 mM Hepes, pH 7.5, and the reactions were initiated by addition of ATP (100 μ M final concentration) following a 20 min preincubation. The initial rates of phosphopeptide formation were measured over 20 min using a Tecan Safire microplate reader with wavelength settings of 360 nm for excitation and 485 nm for emission. The inhibitors were shown to be ATP-competitive from kinetic and crystallographic studies. The K_i values were calculated by fitting the data to the equation for competitive inhibition using nonlinear regression method (GraphPad Prism, GraphPad Software, San Diego, CA) and experimentally measured ATP $K_m = 56 \mu$ M.

Cellular Kinase Phosphorylation ELISA Assays^{10a}. All experiments were done under standard conditions (37 °C and 5% CO₂). IC₅₀ values were calculated by concentration–response curve fitting using a Microsoft Excel based four-parameter method. Cells were seeded in 96-well plates in medium supplemented with 10% fetal bovine serum (FBS) and transferred to serum-free medium [with 0.04% bovine serum albumin (BSA)] after 24 h. In experiments investigating ligand-dependent RTK phosphorylation, corresponding growth factors were added for up to 20 min. After incubation of cells with an inhibitor for 1 h and/or appropriate ligands for the designated times, cells were washed once with HBSS supplemented with 1 mmol/L Na₃VO₄, and protein lysates were generated from cells. Subsequently, phosphorylation of selected protein kinases was assessed by a sandwich ELISA method using specific capture antibodies used to coat 96-well plates and a detection antibody specific for phosphorylated tyrosine residues. Antibody-coated plates were (a) incubated in the presence of protein lysates at 4 °C overnight, (b) washed seven times in 1% Tween 20 in PBS, (c) incubated in a horseradish peroxidase conjugated anti-total-phosphotyrosine (PY-20) antibody (1:500) for 30 min, (d) washed seven times again, (e) incubated in 3,3',5,5'-tetramethylbenzidine peroxidase substrate (Bio-Rad) to initiate a colorimetric reaction that was stopped by adding 0.09 N H₂SO₄, and (f) measured for absorbance in 450 nm using a spectrophotometer. Cell lines used for individual kinases include A549 for c-MET, Karpas 299 for ALK, 3T3-ROn for RON, 293-AXL for AXL, 3T3-E/TIE2 for TIE2, PAE-TRKA for TRKA, PAE-TRKB for TRKB, BaF3-BCL-ABL for ABL, 293-hIR for IR, and Jurkat for LCK.

Human Microsomal Stability Studies. Compounds (1 μ M) were incubated at 37 °C for 30 min in a final volume of 200 μ L of 100 mM potassium phosphate buffer (pH 7.4) containing pooled human liver microsomes (0.8 mg/mL protein) and 2 mM NADPH. Reactions were initiated with the addition of NADPH following a 10 min preincubation. Aliquots of incubation samples were protein precipitated with cold methanol containing 0.1 μ M buspirone (internal standard) and centrifuged, and supernatants were analyzed by LCMS/MS. All incubations were performed in triplicate, and the percent remaining of parent drug at the end of incubation was determined by LCMS/MS peak area ratio.

Cocrystal Structures. c-MET cocrystals were obtained at 13 °C by the hanging drop vapor diffusion method by mixing 1.2 μ L of protein solution (containing 7–13 mg/mL c-MET KD (residues 1051–1348) with a 5-fold molar excess of either crizotinib or 3) with 1.2 μ L of solution containing 0.05 M citrate–phosphate, pH 4.6, 0–0.275 M NaCl, and 21% polyethylene glycol (MW = 3350). Details of the crystal structure determinations can be accessed from the PDB codes 2wgj and

2wkm. The crizotinib and compound 3 cocrystal structures were refined to resolution limits of 2.0 and 2.2 Å, respectively.

AUTHOR INFORMATION

Corresponding Author

*Phone: 858-638-6333. Fax: 877-481-1783. E-mail: jean.cui@pfizer.com.

ACKNOWLEDGMENT

We are grateful to Dr. Nikolaus Schiering for generating the first cocrystal structure of PHA-665752 bound to c-MET, to Muhammad Alimuddin for analytical support, to the Pfizer PDM group for metabolic stability studies, to Dr. Klaus Dress for discussions and making Figures 6 and 7, and to Dr. Beth Lunney for c-MET/ALK sequence identity analyses.

ABBREVIATIONS USED

c-MET, mesenchymal–epithelial transition factor; HGF, hepatocyte growth factor; HGFR, hepatocyte growth factor receptor; ALK, anaplastic lymphoma kinase; RTK, receptor tyrosine kinase; c-KIT, proto-oncogene tyrosine-protein kinase kit; BCR, breakpoint-cluster region; ABL, Abelson leukemia; NSCLC, non-small-cell lung cancer; GIST, gastrointestinal stromal tumor; RCC, renal cell carcinoma; EGFR, epidermal growth factor receptor; VHL, Von Hippel–Lindau; VEGF, vascular endothelial growth factor; LTK, leukocyte tyrosine kinase; IR, insulin receptor; NPM, nucleophosmin; EML4, echinoderm microtubule associated protein-like 4; SBDD, structure based drug design; KD, kinase domain; A-loop, activation loop; FGFR1K, fibroblast growth factor receptor 1 kinase; PDGFR, platelet derived growth factor receptor; LCK, lymphocyte specific kinase; AXL, tyrosine-protein kinase receptor UFO (AXL gene); TIE2, tyrosine kinase with Ig; TRKA, tropomyosin receptor kinase A; TRKB, tropomyosin receptor kinase B; RON, receptor d'origine nantais; ADME, absorption, distribution, metabolism, and excretion; ALCL, anaplastic large cell lymphoma

REFERENCES

- (1) (a) Gschwind, A.; Fischer, O. M.; Ullrich, A. The discovery of receptor tyrosine kinases: targets for cancer therapy. *Nat. Rev. Cancer* **2004**, *4*, 361–370. (b) Krause, D. S.; Van Etten, R. A. Tyrosine kinases as targets for cancer therapy. *N. Engl. J. Med.* **2005**, *353*, 172–187.
- (2) (a) Maulik, G.; Shrikhande, A.; Kijima, T.; Ma, P. C.; Morrison, P. T.; Salgia, R. Role of the hepatocyte growth factor receptor, c-MET, in oncogenesis and potential for therapeutic inhibition. *Cytokine Growth Factor Rev.* **2002**, *13*, 41–59. (b) Ma, P. C.; Maulik, G.; Christensen, J.; Salgia, R. c-MET: structure, functions and potential for therapeutic inhibition. *Cancer Metastasis Rev.* **2003**, *22*, 309–325. (c) Christensen, J.; Burrows, J.; Salgia, R. c-MET as a target in human cancer and characterization of inhibitors for therapeutic intervention. *Cancer Lett.* **2005**, *225*, 1–26. (d) Benvenuti, S.; Comoglio, P. M. The met receptor tyrosine kinase in invasion and metastasis. *J. Cell. Physiol.* **2007**, *213*, 316–325. (e) Knudsen, B. S.; Vande Woude, G. Showering c-MET-dependent cancers with drugs. *Curr. Opin. Genet. Dev.* **2008**, *18*, 87–96.
- (3) (a) Cheng, H.-L.; Trink, B.; Tzai, T.-S.; Liu, H.-S.; Chan, S.-H.; Ho, C.-L.; Sidransky, D.; Chow, N.-H. Overexpression of c-MET as a prognostic indicator for transitional cell carcinoma of the urinary bladder: a comparison with p53 nuclear accumulation. *J. Clin. Oncol.* **2002**, *20*, 1544–1550. (b) Lengyel, E.; Prectel, D.; Resau, J. H.; Gauger, K.; Welk, A.; Lindemann, K.; Salanti, G.; Richter, T.; Knudsen, B.; Vande Woude, G. F.; Harneck, N. c-MET overexpression in node-positive

breast cancer identifies patients with poor clinical outcome independent of Her2/neu. *Int. J. Cancer* **2005**, *113*, 678–682. (c) Lo Muzio, L.; Farina, A.; Rubini, C.; Coccia, E.; Capogreco, M.; Colella, G.; Leonardi, R.; Campisi, G.; Carinci, F. Effect of c-MET expression on survival in head and neck squamous cell carcinoma. *Tumor Biol.* **2006**, *27*, 116–121. (d) Sawada, K.; Radjabi, A. E.; Shinomiya, N.; Kistner, E.; Kenny, H.; Becker, A. R.; Turkyilmaz, M. A.; Salgia, R.; Yamada, S. D.; Vande Woude, G. F.; Tretiakova, M. S.; Lengyel, E. c-MET overexpression is a prognostic factor in ovarian cancer and an effective target for inhibition of peritoneal dissemination and invasion. *Cancer Res.* **2007**, *67*, 1670–1679. (e) Drebber, U.; Baldus, S. E.; Nolden, B.; Grass, G.; Bollschweiler, E.; Dienes, H. P.; Hölscher, A. H.; Mönig, S. P. Overexpression of c-MET as a prognostic indicator for gastric carcinoma compared to p53 and p21 nuclear accumulation. *Oncol. Rep.* **2008**, *19*, 1477–1483.

(4) Morris, S. W.; Kirstein, M. N.; Valentine, M. B.; Dittmer, K. G.; Shapiro, D. N.; Saltman, D. L.; Look, A. T. Fusion of a kinase gene, ALK, to a nucleolar protein gene, NPM, in non-Hodgkin's lymphoma. *Science* **1994**, *263*, 1281–1284.

(5) Bischof, D.; Pulford, K.; Mason, D. Y.; Morris, S. W. Role of the nucleophosmin (NPM) portion of the non-Hodgkin's lymphoma-associated NPM-anaplastic lymphoma kinase fusion protein in oncogenesis. *Mol. Cell. Biol.* **1997**, *17*, 2312–2325.

(6) Palmer, R. H.; Vernersson, E.; Grabbe, C.; Hallberg, B. Anaplastic lymphoma kinase: signalling in development and disease. *Biochem. J.* **2009**, *420*, 345–361.

(7) (a) Soda, M.; Choi, Y. L.; Enomoto, M.; Takada, S.; Yamashita, Y.; Ishikawa, S.; Fujiwara, S.; Watanabe, H.; Kurashina, K.; Hatanaka, H.; Bando, M.; Ohno, S.; Ishikawa, Y.; Aburatani, H.; Niki, T.; Sohara, Y.; Sugiyama, Y.; Mano, H. Identification of the transforming EML4-ALK fusion gene in non-small cell lung cancer. *Nature* **2007**, *448*, 561–566. (b) Rikova, K.; Guo, A.; Zeng, Q.; Possemato, A.; Yu, J.; Haack, H.; Nardone, J.; Lee, K.; Reeves, C.; Li, Y.; Hu, Y.; Tan, Z.; Stokes, M.; Sullivan, L.; Mitchell, J.; Wetzel, R.; MacNeill, J.; Ren, J. M.; Yuan, J.; Bakalarski, C. E.; Villen, J.; Kornhauser, J. M.; Smith, B.; Li, D.; Zhou, X.; Gygi, S. P.; Gu, T.-L.; Polakiewicz, R. D.; Rush, J.; Comb, M. J. Global survey of phosphotyrosine signaling identifies oncogenic kinases in lung cancer. *Cell* **2007**, *131*, 1190–1203.

(8) Soda, M.; Takada, S.; Takeuchi, K.; Choi, Y. L.; Enomoto, M.; Ueno, T.; Haruta, H.; Hamada, T.; Yamashita, Y.; Ishikawa, Y.; Sugiyama, Y.; Mano, H. A mouse model for EML4-ALK-positive lung cancer. *Proc. Natl. Acad. Sci. U.S.A.* **2008**, *105*, 19893–19897.

(9) (a) Caren, H.; Abel, F.; Kogner, P.; Martinsson, I. High incidence of DNA mutations and gene amplifications of the ALK gene in advanced sporadic neuroblastoma tumors. *Biochem. J.* **2008**, *416*, 153–159. (b) Mossé, Y. P.; Laudenslager, M.; Longo, L.; Cole, K. A.; Wood, A.; Attiyeh, E. F.; Laquaglia, M. J.; Sennett, R.; Lynch, J. E.; Perri, P.; Laureys, G.; Speleman, F.; Kim, C.; Hou, C.; Hakonarson, H.; Turkamani, A.; Schork, N. J.; Brodeur, G. M.; Tonini, G. P.; Rappaport, E.; Devoto, M.; Maris, J. M. Identification of ALK as a major familial neuroblastoma predisposition gene. *Nature* **2008**, *455*, 930–935. (c) Janoueix-Lerosey, I.; Lequin, D.; Brugieres, L.; Ribeiro, A.; de Pontual, L.; Combaret, V.; Raynal, V.; Alain Puisieux, A.; Schliepacher, G.; Pierron, G.; Valteau-Couanet, D.; Frebourg, T.; Michon, J.; Lyonnet, S.; Amiel, J.; Delattre, O. Somatic and germline activating mutations of the ALK kinase receptor in neuroblastoma. *Nature* **2008**, *455*, 967–970. (d) Chen, Y.; Takita, J.; Choi, Y. L.; Kato, M.; Ohira, M.; Sanada, M.; Wang, Li.; Soda, M.; Kikuchi, A.; Igarashi, T.; Nakagawara, A.; Hayashi, Y.; Mano, H.; Ogawa, S. Oncogenic mutations of ALK kinase in neuroblastoma. *Nature* **2008**, *455*, 971–974. (e) George, R. E.; Sanda, T.; Hanna, M.; Frohling, S.; Luther, W., 2nd; Zhang, J.; Ahn, Y.; Zhou, W.; London, W. B.; McGrady, P.; Xue, L.; Zozulya, S.; Gregor, V.; Webb, T. R.; Nathanael S. Gray, N. S.; Gilliland, D. G.; Diller, L.; Greulich, H.; Stephan W. Morris, S. W.; Meyerson, M.; Look, A. T. Activating mutations in ALK provides a therapeutic target in neuroblastoma. *Nature* **2008**, *455*, 975–978.

(10) (a) Zou, H. Y.; Li, Q.; Lee, J. H.; Arango, M. E.; McDonnell, S. R.; Yamazaki, S.; Koudriakova, T. B.; Alton, G.; Cui, J. J.; Kung, P.-P.; Nambu, M. D.; Los, G.; Bender, B. L.; Mroczkowski, B.; Christensen, J. G. An orally available small-molecule inhibitor of c-MET, PF-2341066,

exhibits cytoreductive antitumor efficacy through antiproliferative and antiangiogenic mechanisms. *Cancer Res.* **2007**, *67*, 4408–4417. (b) Christensen, J. G.; Zou, H. Y.; Arango, M. E.; Li, Q.; Lee, J. H.; McDonnell, S. R.; Yamazaki, S.; Alton, G.; Mroczkowski, B.; Christensen, J. G. Cytoreductive antitumor activity of PF-2341066, a novel inhibitor of anaplastic lymphoma kinase and c-MET, in experimental models of anaplastic large-cell lymphoma. *Mol. Cancer Ther.* **2007**, *6*, 3314–3322.

(11) McDermott, U.; Iafrate, A. J.; Gray, N. S.; Shioda, T.; Classon, M.; Maheswaran, S.; Zhou, W.; Choi, H. G.; Smith, S. L.; Dowell, L.; Ulkus, L. E.; Kuhlmann, G.; Greninger, P.; Christensen, J. G.; Haber, D. A.; Settleman, J. Genomic alterations of anaplastic lymphoma kinase may sensitize tumors to anaplastic lymphoma kinase inhibitors. *Cancer Res.* **2008**, *68*, 3389–3395.

(12) Sun, L.; Liang, C.; Shirazian, S.; Zhou, Y.; Miller, T.; Cui, J.; Fukuda, J. Y.; Chu, J.-Y.; Nematalla, A.; Wang, X.; Chen, H.; Sistla, S.; Luu, T. L.; Tang, F.; Wei, J.; Tang, C. Discovery of 5-[5-fluoro-2-oxo-1,2-dihydroindol-(3Z)-ylidenemethyl]-2,4-dimethyl-1H-pyrrole-3-carboxylic acid (2-diethylaminoethyl)amide, a novel tyrosine kinase inhibitor targeting vascular endothelial and platelet-derived growth factor receptor tyrosine kinase. *J. Med. Chem.* **2003**, *46*, 1116–1119.

(13) (a) Cui, J. J. Unpublished results. (b) Cui, J.; Zhang, R.; Shen, H.; Chu, J. Y.; Zhang, F.-J.; Koenig, M.; Do, S. H.; Li, X.; Wei, C. C.; Tang, P. C. Preparation of 4-Aryl Substituted Indolinones as Protein Kinase Signal Transduction Modulators for Inhibiting Abnormal Cell Proliferation. PCT Int. Appl. WO2002055517, 2002. (c) Cui, J.; Ramphal, Y.; Liang, C.; Sun, L.; Wei, C. C.; Tang, P. C. Preparation of 5-Aralkylsulfonyl-3-(pyrrol-2-ylmethylidene)-2-indolinone Derivatives as Kinase Inhibitors. PCT Int. Appl. WO2002096361, 2002.

(14) Ryckmans, T.; Edwards, M. P.; Hornea, V. A.; Correia, A. M.; Owena, D. R.; Thompson, L. R.; Trana, I.; Tuttle, M. F.; Young, T. Rapid assessment of a novel series of selective CB2 agonists using parallel synthesis protocols: a lipophilic efficiency (LipE) analysis. *Bioorg. Med. Chem. Lett.* **2009**, *19*, 4406–4409.

(15) Edwards, M. P.; Price, D. A. Role of physicochemical properties and lipophilic ligand efficiency (LipE or LLE) in addressing drug safety risks. *Annu. Rep. Med. Chem.* **2010**, *45*, 381–391.

(16) Wang, X.; Le, P.; Liang, C.; Chan, J.; Kiewlich, D.; Miller, T.; Harris, D.; Sun, Li; Rice, A.; Vasile, S.; Blake, R. A.; Howlett, A. R.; Patel, N.; McMahon, G.; Lipson, K. E. Potent and selective inhibitors of the Met [hepatocyte growth factor/scatter factor (HGF/SF) receptor] tyrosine kinase block HGF/SF-induced tumor cell growth and invasion. *Mol. Cancer Ther.* **2003**, *2*, 1085–1092.

(17) (a) Christensen, J. G.; Schreck, R.; Burrows, J.; Kuruganti, P.; Chan, E.; Le, P.; Chen, J.; Wang, X.; Ruslim, L.; Blake, R.; Lipson, K. E.; Ramphal, J.; Do, S.; Cui, J. J.; Cherrington, J. M.; Mendel, D. B. A selective small molecule inhibitor of c-MET kinase inhibits c-MET-dependent phenotypes in vitro and exhibits cytoreductive antitumor activity in vivo. *Cancer Res.* **2003**, *63*, 7345–7355. (b) Hov, H.; Utne Holt, R.; Baade Rø, T.; Fagerli, U.-M.; Hjorth-Hansen, H.; Baykov, V.; Christensen, J. G.; Waage, A.; Sundan, A.; Børset, M. A selective c-MET inhibitor blocks an autocrine hepatocyte growth factor growth loop in ANBL-6 cells and prevents migration and adhesion of myeloma cells. *Clin. Cancer Res.* **2004**, *10*, 6686–6694.

(18) (a) Engelman, J. A.; Zejnullahu, K.; Mitsudomi, T.; Youngchul Song, Y.; Hyland, C.; Park, J. O.; Lindeman, N.; Gale, C.-M.; Zhao, X.; Christensen, J.; Kosaka, T.; Holmes, A. J.; Rogers, A. M.; Cappuzzo, F.; Mok, T.; Lee, C.; Bruce E. Johnson, B. E.; Cantley, L. C.; Pasi, A.; Jänne, P. A. MET amplification leads to gefitinib resistance in lung cancer by activating ERBB3 signaling. *Science* **2007**, *316*, 1039–1043. (b) Smolen, G. A.; Sordella, R.; Muir, B.; Mohapatra, G.; Barmettler, A.; Archibald, H.; Kim, W. J.; Okimoto, R. A.; Bell, D. W.; Sgroi, D. C.; Christensen, J. G.; Settleman, J.; Haber, D. A. Amplification of Met may identify a subset of cancers with extreme sensitivity to the selective tyrosine kinase inhibitor PHA-665752. *Proc. Natl. Acad. Sci. U.S.A.* **2006**, *103*, 2316–2321. (c) Ma, P. C.; Schaefer, E.; Christensen, J. G.; Salgia, R. A selective small molecule c-MET inhibitor, PHA665752, cooperates with rapamycin. *Clin. Cancer Res.* **2005**, *11*, 2312–2319. (d) Puri, N.; Khramtsov, A.;

Ahmed, S.; Nallasura, V.; Hetzel, J. T.; Jagadeeswaran, R.; Karczmar, G.; Salgia, R. A selective small molecule inhibitor of c-MET, PHA665752, inhibits tumorigenicity and angiogenesis in mouse lung cancer xenografts. *Cancer Res.* **2007**, *67*, 3529–3534. (e) Chattopadhyay, C.; El-Naggar, A. K.; Williams, M. D.; Clayman, G. L. Small molecule c-MET inhibitor PHA665752: effect on cell growth and motility in papillary thyroid carcinoma. *Head Neck* **2007**, *30*, 991–1000. (f) Yang, Y.; Wislez, M.; Fujimoto, N.; Prudkin, L.; Izzo, J. G.; Uno, F.; Ji, L.; Amy, E.; Hanna, A. E.; Langley, R. R.; Liu, D.; Johnson, F. M.; Wistuba, I.; Kurie, J. M. A selective small molecule inhibitor of c-MET, PHA-665752, reverses lung premalignancy induced by mutant *K-ras*. *Mol. Cancer Ther.* **2008**, *7*, 952–960.

(19) Cui, J. J. Unpublished results. PHA-665752 was discovered as a potent and selective c-MET kinase inhibitor. Because of the high lipophilicity and large molecular weight, PHA-665752 demonstrated high metabolic clearance ($CL = 77$ (mL/min)/kg in rat in vivo PK study), low permeability, and a pH dependent solubility. PHA-665752 was originally positioned as a preclinic candidate with an intravenous drug profile. However, the low solubility at pH 7.4 (0.9 $\mu\text{g/mL}$) prevented PHA-665752 as a potential intravenous drug candidate for clinical applications.

(20) Schiering, N.; Knapp, S.; Marconi, M.; Flocco, M. M.; Cui, J.; Perego, R.; Rusconi, L.; Cristiani, C. Crystal structure of the tyrosine kinase domain of the hepatocyte growth factor receptor c-MET and its complex with the microbial alkaloid K-252a. *Proc. Natl. Acad. Sci. U.S.A.* **2003**, *100*, 12654–12659.

(21) Mohammadi, M.; McMahon, G.; Sun, Li.; Tang, C.; Hirth, P.; Yeh, B. K.; Hubbard, S. R.; Schlessinger, J. Structures of the tyrosine kinase domain of fibroblast growth factor receptor in complex with inhibitors. *Science* **1997**, *276*, 955–960.

(22) $LE = [-RT \log(K_i \text{ or } IC_{50})]/\text{number of heavy atoms}$.

(23) Cui, J. J. Unpublished results.

(24) Timofeevski, S. L.; McTigue, M. A.; Ryan, K.; Cui, J.; Zou, H. Y.; Zhu, J. X.; Chau, F.; Alton, G.; Karlicek, S.; Christensen, J. G.; Murray, B. W. Enzymatic characterization of c-MET receptor tyrosine kinase oncogenic mutants and kinetic studies with aminopyridine and triazolopyrazine inhibitors. *Biochemistry* **2009**, *48*, 5339–5349.

(25) Kania, R. S. Structure-Based Design and Characterization of Axitinib. In *Kinase Inhibitor Drugs*; Li, R., Stafford, J. A., Eds.; John Wiley & Sons, Inc.: Hoboken, NY, 2009; pp 167–200.

(26) Wagh, P. K.; Peace, B. E.; Waltz, S. E. Met-related receptor tyrosine kinase Ron in tumor growth and metastasis. *Adv. Cancer Res.* **2008**, *100*, 1–33.

(27) Accornero, P.; Pavone, L. M.; Baratta, M. The scatter factor signaling pathways as therapeutic associated target in cancer treatment. *Curr. Med. Chem.* **2010**, *17*, 2692–2712.

(28) (a) Cheng, H. L.; Liu, H. S.; Lin, Y. J.; Chen, H. H.; Hsu, P. Y.; Chang, T. Y.; Ho, C. L.; Tzai, T. S.; Chow, N. H. Co-expression of RON and MET is a prognostic indicator for patients with transitional-cell carcinoma of the bladder. *Br. J. Cancer* **2005**, *92*, 1906–1914. (b) Catenacci, D. V. T.; Cervantes, G.; Yala, S.; Nelson, E. A.; El-Hashani, E.; Kanteti, R.; El Dinali, M.; Hasina, R.; Brägelmann, J.; Seiwert, T.; Sanicola, M.; Henderson, L.; Grushko, T. A.; Olopade, O.; Karrison, T.; Bang, Y.-J.; Kim, W. H.; Tretiakova, M.; Vokes, E.; Frank, D. A.; Kindler, H. L.; Huet, H.; Salgi, R. RON (MST1R) is a novel prognostic marker and therapeutic target for gastroesophageal adenocarcinoma. *Cancer Biol. Ther.* **2011**, *12*, 9–46.

(29) (a) Drexler, H. G.; Gignac, S. M.; von Wasielewski, R.; Werner, M.; Dirks, W. G. Pathobiology of NPM-ALK and variant fusion genes in anaplastic large cell lymphoma and other lymphomas. *Leukemia* **2000**, *14*, 1533–1559. (b) Cools, J.; Wlodarska, I.; Somers, R.; Mentens, N.; Pedoutour, F.; Maes, B.; De Wolf-Peeters, C.; Pauwels, P.; Hagemeijer, A.; Marynen, P. Identification of novel fusion partners of ALK, the anaplastic lymphoma kinase, in anaplastic large-cell lymphoma and inflammatory myofibroblastic tumor. *Genes, Chromosomes Cancer* **2002**, *34*, 354–362.

(30) Viaud, M.-C.; Jamoneau, P.; Savelon, L.; Guillaumet, G. Synthesis of 6-substituted 2-phenyloxazolo[4,5-*b*]pyridines. *Heterocycles* **1995**, *41*, 2799–2809.

(31) Suh, Y.-G.; Shin, D.-Y.; Cho, K.-H.; Ryu, J.-S. Concise and versatile syntheses of *N*-arylkylpiperidines as potential intermediates for 4-anilidopiperidine analgesics. *Heterocycles* **1998**, *48*, 239–242.

(32) Carlos, A.; Martinez, C. A.; Keller, E.; Meijer, R.; Metselaar, G.; Kruihof, G.; Moore, C.; Kung, P.-P. Biotransformation-mediated synthesis of (1*S*)-1-(2,6-dichloro-3-fluorophenyl)ethanol in enantiomerically pure form. *Tetrahedron: Asymmetry* **2010**, *21*, 2408–2412.

(33) Yamazaki, S.; Skaptason, J.; Romero, D.; Vekich, S.; Jones, H. M.; Tan, W.; Wilner, K.; Koudriakova, T. Prediction of oral pharmacokinetics of cMet kinase inhibitors in humans: physiologically-based pharmacokinetic modeling versus traditional one-compartment model. *Drug Metab. Dispos.* **2011**, *39*, 383–393.

(34) Yamazaki, S.; Skaptason, J.; Romero, D.; Lee, J. H.; Zou, H. Y.; Christensen, J. G.; Koup, J. R.; Smith, B. J.; Koudriakova, T. Pharmacokinetic–pharmacodynamic modeling of biomarker response and tumor growth inhibition to an orally available c-MET kinase inhibitor in human tumor xenograft mouse models. *Drug Metab. Dispos.* **2008**, *36*, 1267–1274.

(35) (a) Kwak, E. L.; Bang, Y.-J.; Camidge, R.; Shaw, A. T.; Solomon, B.; Maki, R. G.; Ou, S.-H. I.; Dezube, B. J.; Jänne, P. A.; Costa, D. B.; Varella-Garcia, M.; Kim, W.-H.; Lynch, T. J.; Fidias, P.; Stubbs, H.; Engelman, J. A.; Sequist, L. V.; Tan, W.; Gandhi, L.; Mino-Kenudson, M.; Wei, G. C.; Shreeve, S. M.; Ratain, M. J.; Settleman, J.; Christensen, J. G.; Haber, D. A.; Wilner, K.; Salgia, R.; Shapiro, G. L.; Clark, J. W.; Iafrate, A. J. Anaplastic lymphoma kinase inhibition in non-small-cell-lung cancer. *N. Engl. J. Med.* **2010**, *363*, 1693–1703. (b) Butrynski, J. E.; D'Adamo, D. R.; Hornick, J. L.; Dal Cin, P.; Antonescu, C. R.; Jhanwar, S. C.; Ladanyi, M.; Capelletti, M.; Rodig, S. J.; Ramaiya, N.; Kwak, E. L.; Clark, J. W.; Wilner, K. D.; Christensen, J. G.; Jänne, P. A.; Maki, R. G.; Demetri, G. D.; Shapiro, G. I. Crizotinib in ALK-rearranged inflammatory myofibroblastic tumor. *N. Engl. J. Med.* **2010**, *363*, 1727–1733. (c) Gambacorti-Passerini, C.; Messa, C.; Pogliani, E. M. Crizotinib in large cell anaplastic lymphoma. *N. Engl. J. Med.* **2011**, *364*, 775–776.

(36) (a) Ou, S.-H. I.; Kwak, E. L.; Siwak-Tapp, C.; Dy, J.; Bergethon, K.; Clark, J. W.; Camidge, D. R.; Solomon, B. J.; Maki, R. G.; Bang, Y.-J.; Kim, D.-W.; Christensen, J.; Tan, W.; Wilner, K. D.; Salgia, R.; Iafrate, A. J. Activity of Crizotinib (PF02341066), a Dual Mesenchymal-Epithelial Transition (MET) and Anaplastic Lymphoma Kinase (ALK) Inhibitor, in a Non-Small Cell Lung Cancer Patient with de novo MET Amplification. *J. Thorac. Oncol.* **2011**, *6*, 942–946. (b) Chi, A. S.; Kwak, E. L.; Clark, J. W.; Wang, D. L.; Louis, D. N.; Iafrate, A. J.; Batchelor, T. Clinical Improvement and Rapid Radiographic Regression Induced by a MET Inhibitor in a Patient with MET-Amplified Glioblastoma. Presented at ASCO 2011 Annual Meeting, Chicago, IL, June 3–7, 2011; Abstract 2072. (c) Lennerz, J. K.; Kwak, E. L.; Michael, M.; Fox, S. B.; Ackerman, A.; Bergethon, K.; Lauwers, G. Y.; Christensen, J. G.; Wilner, K. D.; Haber, D. A.; Salgia, R.; Bang, Y.; Clark, J. W.; Solomon, B. J.; Iafrate, A. J. Identification of a Small and Lethal Subgroup of Esophagogastric Adenocarcinoma with Evidence of Responsiveness to Crizotinib by MET Amplification. Presented at ASCO 2011 Annual Meeting, Chicago, IL, June 3–7, 2011; Abstract 4130.